The functional role of NOTCH and potential NOTCH associated genes in head and neck cancer

Shaoxia Wang

Master's thesis

University of Turku
Faculty of Medicine
Institute of Biomedicine
High-Content Screening Laboratory
FICAN West Cancer Centre Laboratory
08.05.2022

Master's degree in Biomedical Imaging
Specialization theme: Light Microscopy Imaging

Credits: 20 ECTS

Supervisors:
1: Dr Mervi Toriseva
2: Adjunct professor Matthias Nees

The originality of this thesis has been checked in accordance with the University of Turku quality assurance system using the Turnitin Originality Check service.

Abstract

UNIVERSITY OF TURKU

Department of Biomedicine

Faculty of Medicine

SHAOXIA WANG The functional role of NOTCH and potential NOTCH associated genes in head and neck cancer

Master's thesis, 72 pages, 8 Appendices

Specialization level: Light Microscopy Imaging

May 2022

Notch signaling is actively involved in cell differentiation, proliferation, and apoptosis, and plays a significant role in tumor growth and prognosis of head and neck squamous cell carcinoma (HNSCC). Altered NOTCH expression and mutations are often associated with poor prognosis in patients with HNSCC. Rrecently, our group has identified a specific gene expression signature which is likely associated with Notch signaling in HNSCC. From this signature, Dishevelled Segment Polarity Protein 3 (DVL3) and Proteasome 26S Subunit Ubiquitin Receptor, Non-ATPase 2 (PSMD2) were selected and studied in this work. Based on bioinformatic analysis, these two genes are found amplified or over-expressed in about 30-40% of all HNSCC cases. They also showed potential association with Notch mutations in some cancers. The main purpose of this work is to find out experimentally whether there is a regulatory association between DVL3 or PSMD2 and NOTCH signaling. Another purpose of this work is to investigate what are the functional roles of NOTCH and these two genes in HNSCC. The methods used in this work are 2D and organotypic 3D cultures, metabolic cell viability assay, proliferation assay, IncuCyte live cell imaging and confocal imaging with phenotypic image analysis. siRNA transfection, western blotting, and quantitative real-time polymerase chain reaction (qPCR) are also used for gene expression and signaling studies. The results showed that Notch signaling is active in our studied cell lines, and Notch seems to have a tumor promoting role in the cell line studied in this work and inhibition of NOTCH affects cell growth and viability in 2D and 3D cultures. DVL3 may regulate NOTCH1 activity and knocking DVL3 down may increase the cell growth and viability in 3D culture. In addition, PSMD2 is found expressed at significantly higher levels in HNSCC tumors compared to benign tissues.

KEYWORDS: HNSCC, NOTCH, DVL3, PSMD2, FLI06, Yhhu3792, siRNA transfection, 3D organotypic cell culture, viability

LIST OF ABBREVIATIONS

ADAM	A Disintegrin and metalloproteinase domain-containing protein
AMIDA	Automated Morphometric Image Data Analysis software
APP	Amyloid Beta Precursor Protein
AXL	AXL receptor tyrosine kinase
BCA	Bicinchoninic acid
Bcl-2	B-cell lymphoma 2
CRISPR/Cas9	Clustered regularly interspaced palindromic repeats
CSC	Cancer stem cell
CSL	Intracellular effector molecule (DNA binding protein)
DLL	Delta-like ligands
DMSO	Dimethyl Sulfoxide
DVL3	Dishevelled Segment Polarity Protein 3
ECM	Extracellular matrix
EDTA	Ethylenediaminetetraacetic acid
EGFR	Epidermal growth factor receptor
EMT	Epithelial-mesenchymal transition
ER	Endoplasmic reticulum
GLI1	Glioma-associated oncogene
HES	Hairy enhancer of split gene
HEY	Hairy Ears, Y-Linked
HNC	Head and neck cancer
HNSCC	Head and Neck Squamous Cell Carcinoma
HPV	Human papillomavirus
JAG	Jagged
NICD	Notch intracellular domain
NOTCH	Neurogenic locus notch homolog protein
PBS	Phosphate-buffered saline
PD	Patient derived
PD-1	Programmed cell death protein 1

PSMD2	Proteasome 26S Subunit Ubiquitin Receptor, Non-ATPase 2
qPCR	Quantitative real-time polymerase chain reaction
RBPJ	Recombination Signal Binding Protein for Immunoglobulin Kappa J Region
siRNA	Small interfering RNA
TBST/TBS-Tween	A mixture of tris-buffered saline (TBS) (a buffer solution) and Polysorbate 20 (a polysorbate-type nonionic surfactant)
TCGA	The Cancer Genome Atlas
TME	Tumor microenvironment
UT-SCC	University of Turku Squamous Cell Carcinoma
Wwox	WW Domain Containing Oxidoreductase

Table of Contents

1. REVIEW OF THE LITERATURE 1
1.1 Head and neck squamous cell carcinoma 1
1.2 Notch signaling pathway in HNSCC 2
1.3 DVL3 and PSMD2 in HNSCC 5
1.4 Tumor microenvironment and extracellular matrices in vitro 6
1.5 2D and organotypic 3D cultures 8
1.6 Phenotypic analysis of cells in 3D culture 8
2. HYPOTHESIS AND AIMS OF THE STUDY 9
3. MATERIALS AND METHODS 10
3.1 Cell lines and culture conditions 10
3.2 Patient samples 11
3.3 Drug treatments and proliferation assay for the cells in 2D culture 12
3.4 The pipeline for organotypic 3D culture and quantitative analysis 13
3.4.1 Organotypic 3D culture 14
3.4.2 Notch modulation by chemical compounds 15
3.4.3 IncuCyte real-time live cell imaging 15
3.4.4 Spinning disc confocal microscopy 16
3.4.5 Quantitative phenotypic analysis with AMIDA 16
3.5 Cell metabolic viability assay 18
3.6 Harvest protein lysates from cultured cells 18
3.7 RNA isolation from patient samples and cultured cell lines 20
3.8 Western blotting 20
3.9 Primary and secondary antibodies 21
3.10 DVL3 and PSMD2 silencing with siRNA transfection 22
3.11 Quantitative real-time PCR (qPCR) 23
3.12 Statistical analysis 24
4. RESULTS 24
4.1 Analysis of Notch signaling in the cell lines 24

4.2 Functional role of Notch signaling in cancer cell growth and viability in 2D and 3D cultures.....25
4.2.1 The effect of FLI 06 on Notch activity and HNSCC cell function 26
4.2.2 The effect of Yhhu 3792 on Notch activity and HNSCC cell function.....33
4.3 Verification of PSMD2 and DVL3 expressions in cell lines by qPCR and western blot.....39
4.4 Possible regulation of PSMD2/DVL3 expression by Notch signaling 41
4.5 Possible regulation of Notch signaling by PSMD2/DVL3 41
4.6 The effect of DVL3 knock down on cell growth pattern in 2D and 3D culture 43
4.7 Expression of PSMD2 and DVL3 in HNSCC patient samples 45
5. DISCUSSION 46
5.1 Notch activity and expression of DVL3 and PSMD2 in UT-SCC cell lines ...46
5.2 Differential Notch inhibition and activation by drug treatments.....47
5.3 Inhibition of Notch signaling affects cell growth pattern and reduces cell proliferation and viability.....48
5.4 Potential regulation between DVL3/PSMD2 and Notch signaling.....49
5.5 Knocking down of DVL3 affects cell growth and viability 50
5.6 Differential expression of PSMD2 and DVL3 in patient samples 50
6. CONCLUSIONS 51
7. ACKNOWLEDGEMENTS.....52
8. REFERENCES.....53
9. APPENDICES 59

1. REVIEW OF THE LITERATURE

1.1 Head and neck squamous cell carcinoma

Cancer is a group of diseases caused by genetic alterations in the cell and is characterized by uncontrolled cell division with the potential for metastasis (Rahman et al., 2020). Head and neck cancer (HNC) refers to the cancer types which develop from the lip and oral cavity, larynx, pharynx, nose, sinus, salivary glands, or the skin of the face (Auperin, 2020). 90% of HNC are initiated by the epithelial squamous cells that line the mucosal surfaces of the head and neck and are accordingly called squamous cell carcinomas (SCC). Other, less common head and neck cancers are found in the salivary glands, sinuses, muscles, or nerves in HNC, such as mucoepidermoid tumors or sinonasal carcinomas. Head and neck squamous cell carcinomas (HNSCC) are mainly caused by chronic alcohol and/or tobacco use, and a fraction of 15-25% of HNSCC is associated with human papillomavirus (HPV) infection. Globally, 890,000 new cases and 450,000 deaths due to head and neck cancer were reported in 2018 (Chow, 2020). Currently, surgery, chemotherapy, and irradiation, especially the combination of these strategies, are the most common treatments for HNSCC. Advanced, recurrent, and metastatic cancer patients (R/M HNSCC) are often treated by combined chemoradiotherapy. Although the overall five-year survival rate in HNSCC patients has been recently raised to ~65% (Johnson et al., 2020), it is still one of the more aggressive and difficult to treat tumor entities. Specifically, clinical resistance to chemotherapy (e.g., cisplatin-resistant) or chemoradiotherapy, followed by distant metastases or local recurrence, most significantly contributes to poor outcome and prognosis. Therefore, many efforts are undertaken to develop more targeted, such as biomarker-driven targeted therapies. The current approved target therapies for HNSCC are cetuximab (an epidermal growth factor receptor (EGFR) inhibitor) and immune checkpoint inhibitors (nivolumab and pembrolizumab) (Fasano et al., 2021, ClinicalTrials.gov). In addition, Tuomainen et al. found that Navitoxlax (an inhibitor of Bcl-2) irradiation combination results in strong *in vitro* synergistic antitumor effects in HPV-negative HNSCC, which might possess therapeutic potential for HNSCC patients (Tuomainen et al., 2021). Nevertheless, although the current approved targeted therapies, especially immunotherapy, are promising approaches for the treatments of HNSCC, they show very limited benefit for patients. Therefore, new molecular targeted therapies and prognostic biomarkers are urgently needed.

1.2 Notch signaling pathway in HNSCC

The Notch signaling is a highly conserved cell signaling pathway, which is present in almost all multicellular organisms (Artavanis-Tsakonas et al., 1999). There are four different NOTCH receptors in mammals (NOTCH1-4) (Kumar et al., 2016). NOTCH receptors are single transmembrane proteins with extracellular, transmembrane, and intracellular domains. Simultaneously, there are five ligands that bind to the 4 NOTCH receptors: two jagged 1 and 2 ligands (JAG1 and JAG2), and three delta-like ligands DLL1, DLL3 and DLL4. Activation of Notch signaling pathway includes several steps. The Notch receptors are first constitutively cleaved during maturation by Furin-like convertases (S1 cleavage) within the Golgi network and then translocate to the cytomembrane and re-assembled as heterodimeric receptors at the cell surface. The re-assembled Notch receptors are normally triggered through direct cell-to-cell contact, in which the transmembrane proteins of the signal-sending cell form a direct contact via their ligands that bind the NOTCH receptors at the signal-receiving cells (Greenwald, 2012). This induces proteolytic cleavage of the NOTCH receptors at the cell surface by ADAM10 or ADAM17 proteases (S2 cleavage) and gamma secretase (S3 cleavage). The cleaved NOTCH intracellular domains (NICD) are released and enter the cell nucleus and bind to the CSL/RBPJ transcription factor complex, the targeted gene are then expressed (Oswald et al., 2001). A schematic illustration of Notch signaling pathway is shown in Figure 1.

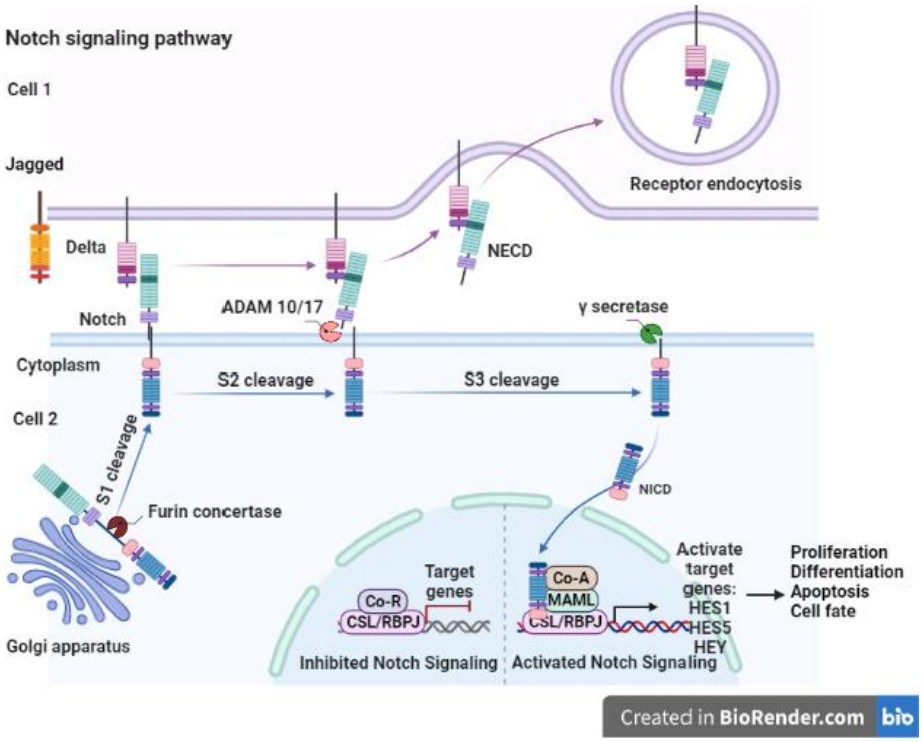

Figure 1. Notch signaling pathway. Cell 1 is the signal sending cell. Cell 2 is the signal receiving cell. Notch signaling pathway can act either in a canonical or non-canonical fashion, depending on whether CSL/RBPJ is involved or not.

The Notch signaling pathway plays a dual role in HNSCC: it can act either as tumor suppressor or as an oncogene/tumor promoter. NOTCH1 is often considered as a tumor suppressor, since it is often mutated and lost its growth- and tumor suppressing function in HNSCC (Sun et al., 2014; *The Cancer Genome Atlas* (TCGA) data/cBioportal). The majority of NOTCH1 mutation identified in HNSCC are loss-of-function, truncating, or nonsense mutations. In contrast, gain-of-function, oncogenic mutations of NOTCH1, which are common in other cancer types like aggressive breast cancers, are rarely observed in HNSCC. Nevertheless, gain-of-function mutations of NOTCH receptors have been observed in HNSCC, often accompanied with over-expression (Sun et al., 2014). In addition, NOTCH1 mutation is often accompanied with simultaneous over expression of JAG1, JAG2 or NOTCH3, along with activation of downstream NOTCH effectors, such as HES1 and HEY1 (Sun et al., 2014). Rettig et al. reported that higher expression of HEY1 was independent of NOTCH1 and is associated with poor patient outcome in HNSCC (Rettig et al., 2018; Misiorek et al., 2021). Various reports show that JAG1 and JAG2 are related to the aggressive behaviour in HNSCC tumor cells (Katoh and Katoh 2020; Sun et al., 2014; Lin et al., 2010). Alterations in NOTCH1 have also been reported

to be associated with tumor invasion in oesophageal SCC and are related to poor prognosis (Natsuizaka et al., 2017; Lubin et al., 2018; Gan et al., 2019). Fukusumi and Califano reported that the NOTCH4-HEY1 pathway is upregulated in HNSCC and over-expression of NOTCH1 affects HNSCC cancer cell proliferation and cisplatin resistance (Fukusumi and Califano, 2018). Other work done by Gan et al. shows that there is an association between NOTCH1 and increased metastatic potential of tongue cancer cells. NOTCH1 is frequently upregulated and promotes the tongue cancer cell proliferation in *in vitro* and in xenograft cancer model. (Gan et al., 2018, 2019). Lee et al. reported that NOTCH1 contributes to the stemness of HNSCC. Downregulation of NOTCH1 signaling attenuates cancer stem cell traits and enhances the cisplatin chemosensitivity to HNSCC cancer stem cells (Lee et al., 2016). Lin et al. showed that high co-expression of JAG1 and NOTCH1 signaling is associated with poor prognosis for the patients with HNSCC (Lin et al., 2010). Wu et al. suggested that NOTCH1 is one of the hub genes involved in regulating the cisplatin resistance of oral squamous cell carcinoma (Wu et al., 2020). At the same time, the true function of NOTCH1 and Notch signaling remains controversial. A study of inactivating NOTCH1 mutations in HNSCC showed that functional NOTCH1 may inhibit tumor growth and proliferation (Shhyam, 2015), and thus act as a tumor suppressor. Loss of NOTCH1 signaling can promote HNSCC tumorigenesis and clinical aggressiveness (Shah et al., 2020). Likewise, it was found that CRISPR-Cas9 knock out of NOTCH1 and NOTCH2 in wild-type HNSCC cells results in an increased cell growth (Shhyam, 2015).

Notch signaling is also found fundamentally involved in epithelial maturation or differentiation programmes. Epithelial differentiation is considered opposing to the aggressive invasion of epithelial cancer cells, including HNSCC (Misiorek et al., 2021, Kalafut et al., 2021). It is not clear if and how Notch signaling modulates tumor cell motility and invasion. However, it is well established that Notch signaling can induce or promote epithelial-to-mesenchymal transition (EMT), a trans-differentiation process that shows a high degree of tumor cell plasticity (Mutvei et al., 2018, reviewed in detail in Kalafut et al. 2021).

The significance of Notch signaling in carcinogenesis and prognosis of HNSCC, despite the still somewhat controversial function of NOTCH mutations in different studies, makes

it a potential target for new therapies, especially since high NOTCH expression was often associated with poor prognosis in patients with HNSCC.

1.3 DVL3 and PSMD2 in HNSCC

DVL3 (Dishevelled Segment Polarity Protein 3) is one member of dishevelled proteins, which bridges the receptors and downstream targets as a cytoplasmic scaffold protein (Wang et al., 2018; Zhao et al., 2020). It is a cardinal upstream regulator of Wnt-signaling and also a member of the Notch signaling pathway. Notch signaling can closely crosstalk with Wnt signaling through DVL3, although it is not entirely clear which direction this crosstalk takes (Zhao et al., 2020). DVL3 has been linked to recurrence prediction or treatment responses in prostate and colorectal cancers (Zhao et al., 2020). It was also reported that DVL3 silencing increased the drug response and attenuated the activated Notch signaling and stemness in colorectal cancer by down-regulating NOTCH intracellular domain and its downstream targets (Zhao et al., 2020). Collu et al. found that Wnt inhibited Notch signaling through Dishevelled which bound and directly inhibited CLS transcription factors downstream of NOTCH receptors. The crosstalk between Notch and Wnt regulated cell-fate specification *in vivo* (Collu et al., 2012). In prostate cancer, DVL3 was found to be involved in regulating cancer cell stemness and progression by activating Wnt signaling (Pai et al., 2019). The expression of DVL proteins in HNSCC was recently studied by Celebi et al. who reported that there is higher expression of DVL1 and DVL3 in cancer cell lines compared to normal (Celebi et al., 2020).

PSMD2 (Proteasome 26S Subunit Ubiquitin Receptor, Non-ATPase 2) is an essential part of a regulatory subunit in the 26S proteasome complex which belongs to the ubiquitin-proteasome system. The 26S proteasome is a multiprotein complex found in both the cytoplasm and the nucleus of eukaryotic cells and plays a pivotal role in maintaining normal cellular functions (Frankland-Searby and Bhaumik, 2021). It has two main subcomplexes, the 20S core and 19S regulatory complex. The proteasome regulates cellular protein turnover through binding of ubiquitylated proteins to the 19S regulatory complex with subsequent catalytic degradation in the 20S core complex (Rubio et al. 2021; Livneh et al., 2016; Tanaka, 2009). Abnormal expression of PSMD2 has been found in

lung adenocarcinoma, breast cancer, hepatocellular carcinoma as well as head and neck cancer (Tan et al., 2019; Reddy et al., 2019; Li et al., 2018; Matsuyama et al., 2011). Several anti-cancer drugs were developed to inhibit the 26S proteasome to treat multiple cancers (Frankland-Searby and Bhaumi, 2021). However, there are adverse effects and drug resistance which raises the need for alternative therapies. Recently, PSMD2 was suggested as an independent predictor or prognostic biomarker for urothelial bladder carcinoma (Salah Fararjeh et al., 2021). A comprehensive analysis of ubiquitin-proteasome system genes, including PSMD2, related to prognosis and immunosuppression in HNSCC was carried out by Wang et al. by constructing a prognostic risk model (Wang et al., 2021).

Based on bioinformatic data mining, both DVL3 and PSMD2 are frequently amplified and/or upregulated in many HNSCC (TCGA data set, cBioPortal database). High expression of PSMD2 and DVL3 are found to be associated with poor patient survival (The Human Protein Atlas). However, it was not clear if and in which direction both proteins may be linked to Notch pathway activity and Notch downstream signaling. It was also hypothesized that DVL3 and PSMD2 may be upstream regulators of NOTCH1/3 expression and could thus promote or modulate Notch signaling in HNSCC cancer cells.

1.4 Tumor microenvironment and extracellular matrices in vitro

The tumor microenvironment (TME) is the environment surrounding the tumor cells and tumor tissue, it mainly contains blood vessels, fibroblasts, immune cells, secreted growth factors and signaling molecules, as well as the extracellular matrix (ECM). The ECM is a three-dimensional macromolecular network which provides structural support for tissues and organs (Cox, 2021). The main components are laminins, collagens, enzymes, elastin, proteoglycans, hydroxyapatite, glycoproteins, and various growth factors. The ECM components play an important role in regulating cell differentiation, proliferation, migration, survival, and adhesion (Hagemann et al., 2017). The Notch signaling pathway can directly or indirectly interact with components of the tumor microenvironment (LaFoya et al., 2016; Misiorek et al., 2021), such as stromal fibroblasts, endothelial cells, and a spectrum of immune cells. However, it is poorly established how TME and ECM contribute to, or modulate Notch signaling activities in tumors, and which consequences

this may have on tumor growth and proliferation, differentiation, and aggressive behaviour or chemosensitivity.

The extracellular matrices that have been developed for application in 3D cultures include synthetic scaffolds and biological matrices originated from animals. One commercial and widely used animal derived matrix is Matrigel. However, the disadvantage of using biological matrices is the variation between the batches. Since the most abundant proteins in ECM are typically collagens, rodent-derived collagens such as collagen Type I is also commonly used in *in vitro* studies. In addition, human-derived matrices, such as Myogel, fibronectin, and fibrinogen are also developed and used as matrices (Salo et al., 2015; Mao and Schwarzbauer, 2005; Pereira et al., 2002).

In this work, Matrigel and Myogel were used as biologically relevant ECM gels for organotypic 3D cultures. Matrigel is a laminin/collagen IV-rich basement membrane extracellular matrix which is secreted by Engelbreth-Holm-Swarm mouse sarcoma cells and produced by Corning Life Sciences (https://en.wikipedia.org/wiki/Matrigel). Besides the major basement membrane components, such as laminin, entactin, and type IV collagen, it may also contain growth factors including EGF, beta and insulin-like, and transforming growth factors (Hughes et al., 2010). Myogel is a human-based extracellular matrix containing human tumor environment components including collagen, laminin, cytokines, and growth factors (Salo et al., 2015). It was extracted from human benign tumor tissue called "leiomyoma" and developed in Professor Tuula Salo's group at the University of Oulu, Finland (Salo et al., 2015). Myogel has an advantage over Matrigel, that is, it better mimics the human tumor microenvironment providing more relevant aspects of interaction between cancer cells and human tumor microenvironment (Tuomainen et al., 2020). Both Matrigel and Myogel contain the basic ECM components including laminin, collagen IV, heparan sulphate proteoglycans, nidogen and EFG growth factor, except that in Matrigel there is no tenascin-C, collagen XII and XIV (Salo et al., 2015). The main difference between Matrigel and Myogel is that Myogel contains less laminins than Matrigel. Laminins are well known to promote cell differentiation but repress tumor cell motility. In addition, in comparison with Matrigel, Myogel is superior in enhancement of cancer cell proliferation, migration and invasion (Salo et al., 2015).

1.5 2D and organotypic 3D cultures

Organotypic 3D models have become more attractive and considered more biological relevant than 2D monolayer cultures on plastic (Härmä et al., 2010; Härmä et al., 2014). 2D culture allows biologist to observe and manipulate the cells but it cannot provide the cell-cell and cell-ECM interactions information due to the absence of physiological ECM on artificial plastics (Härmä et al., 2010; Härmä et al., 2014). Organotypic 3D models allow the spontaneous formation of complex, tissue-like structures after embedding single normal or tumor cells into supportive ECM (Åkerfelt et al., 2017). It can mimic more faithfully the physiological environment of a patient tumor compared to conventional 2D cultures on plastic. (Härmä et al., 2010; Härmä et al., 2014).

1.6 Phenotypic analysis of cells in 3D culture

Advanced phenotypic image analysis tools have been widely established for cells in 2D cultures (Åkerfelt et al.,2017). For example, KNIME and CellProfiler are open-source software specifically tailored for high-content analyses of microscopic images for single cells in 2D conditions (Stöter et al., 2013). The most common used open-source software for single cell analysis in 3D multicellular culture is IT3DImageJ Suite (ImageJ). Other open-source software programs, to name a few, including OpenSegSPIM, Real-time accurate cell-shape extractor (RACE) which is mainly for confocal/multiphoton/LSFM image analysis (Piccinini et al., 2020); VoxelView (SGI Vital Images, Imaris), Metamorph (Molecular Devices), Analysis (Olympus, OSIS), and Volocity (PerkinElmer) are mainly specialized for detailed analysis of tissue-like histology and a few selected 3D organoids (Megason and Fraser, 2003 and 2007; Åkerfelt et al., 2017). Our lab has developed an automated image analysis software called AMIDA (Automated Morphometric Image Data Analysis) which has been proven to be a useful tool for an automated quantification of large numbers of images and structures from complex and organotypic cultures. It supports high-content screens at large scale and can also be combined with quality control and statistical tools for data annotation and visualization (Härmä et al., 2014). AMIDA has been successfully used in our lab as a high-content image analysis approach for quantitative analysis of the dynamic morphological drug responses/chemosensitivity in 3D organotypic cell cultures (Härmä et al., 2014; Ahonen et al., 2017, Åkerfelt et al.,2015; Åkerfelt et al., 2017). It is user-friendly, straightforward

and facilitates cell-based organotypic 3D assays in basic research, early-stage drug discovery, and pharmacological target validation (Åkerfelt et al., 2017).

2. HYPOTHESIS AND AIMS OF THE STUDY

In the PESCADORE AoF consortium (309373), we recently identified that the knock-out of NOTCH1 and NOTCH3 receptors in breast cancer cell lines results in a specific gene expression pattern. Knockout of Notch1 and Notch 3 significantly affects the morphology in 3D cultures suggesting changed cell motility and invasion (PESCADOR consortium, unpublished). Based on detailed bioinformatic analyses (unpublished) of several public data sets, in addition to previously mentioned gene expression data, an independent gene signature with potential functional association with NOTCH signaling, was identified in our group. From these genes, over 50 candidate genes were found altered in more than 30% of HNSCC cases and cell lines (TCGA, Firehose Legacy, cBioportal). Any functional association of these amplified and over-expressed genes with Notch signaling is unknown, but plausible, based on their original selection criteria. The thesis project, therefore, focused on functional validation of two selected candidate genes, namely, PSMD2 and DVL3. These genes also showed the highest frequency of overexpression and amplification in HNSCC.

PSMD2 is an essential part of a regulatory subunit in a proteasome S26. DVL3 is an intracellular mediator of Wnt signaling and is associated to cell proliferation and tumor growth. However, the precise role of DVL3 and PSMD2 in HNSCC is currently unknown. My primary hypotheses in this study are that these genes play a significant role in regulating and modulating the aggressiveness of HNSCC, and their expression may either be regulated by Notch signaling, or vice versa: these genes may contribute to the regulation of NOTCH1 and NOTCH3 expression in HNSCC tumor cells. Moreover, provided a clear difference in the expression of these genes in patient tumor samples compared to benign tissues could be validated, these genes could provide as prognostic biomarkers to better predict treatment outcomes or prognosis, especially of advanced HNSCC patients. The assumed correlation between DVL3/PSMD2 and Notch signaling may also be relevant for personalized cancer medicine, in which Notch pathway activity

has been suggested as a predictive factor. Thus, the objectives of this thesis work are to investigate experimentally:

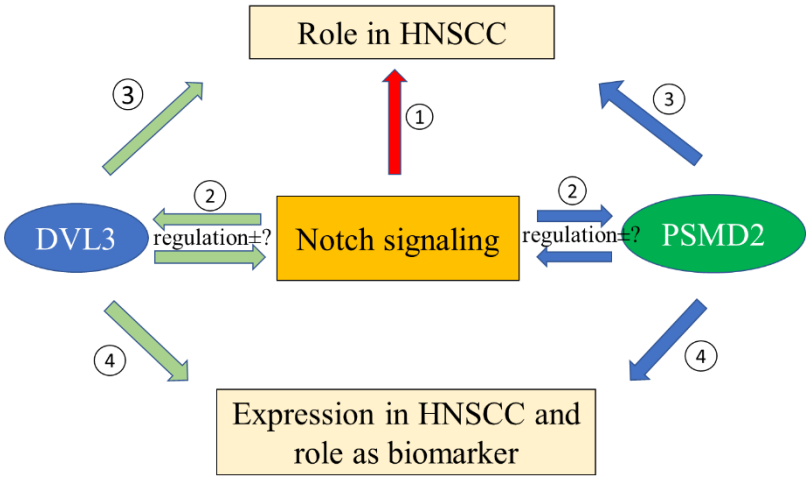

1. whether Notch signaling is active in the studied UT-SCC cell lines and does it play a functional role in cell growth and viability.
2. whether there is a regulatory association between DVL3 and PSMD2 expression and NOTCH expression or its molecular functions.
3. how does knock-down of DVL3 or PSMD2 affect the tumor cell growth and aggressive behavior in 2D and 3D culture.
4. analysis of the expression of DVL3 and PSMD2 in HNSCC patient samples and what may be their potential use as prognostic biomarkers.

3. MATERIALS AND METHODS

3.1 Cell lines and culture conditions

The HNSCC cell lines used in this thesis work were UT-SCC-24A (primary tongue squamous cell carcinoma), UT-SCC-24B (metastatic tongue squamous cell carcinoma), UT-SCC-42A (primary laryngeal carcinoma), and UT-SCC-42B (metastatic laryngeal carcinoma), which were established by Professor Grenman at the University of Turku (Department of Otolaryngology, Turku University, Turku, Finland) (Grenman et al., 1992). All the cell lines were first revived from frozen ampoules (stored at -150 ºC) and cultured in DMEM (Gibco™/Invitrogen, Tokyo, Japan) supplemented with 2 mM

GlutamaxTM-I, 10% heat-inactivated fetal bovine serum (hi-FBS), 1% antibiotics (Penicillin-Streptomycin (Life Technologies)) and 0.025 µM hydrocortisone (Sigma-Aldrich, St. Louis, Mo, USA). All cells were propagated at 37ºC in standard cell culture conditions (5% CO_2, 95% humidity) and subcultured at ~70-90% confluence. The medium was changed every 2 or 3 days. These cell lines were selected based on their suggested invasive potential in organotypic 3D cultures, and the absence of inactivating/truncating NOTCH1 or NOTCH3 mutations. UT-SCC 42A and 24A have been experimentally confirmed and validated not harbour inactivating (loss-of-function) NOTCH mutations nor amplification and/or overexpression of NOTCH1 and 3 (Lepikhova et al., 2018).

3.2 Patient samples

Freshly isolated patient samples were received from primary HNSCC tumors and corresponding benign tissues through our clinical collaborators at the Otorhinolaryngology clinic in Turku University Hospital. After informed patient consent was received, fresh tumor tissue samples were collected during scheduled surgery. The study was approved by the regional Ethics Committee of the Hospital District of Southwest Finland Turku (Dnro 166/1801/2015) and was carried out according to the Declaration of Helsinki. After arrival in the laboratory, the samples were snap frozen in liquid nitrogen for 10-15 min and stored to -80 ºC. The list of received patient samples is shown in Table 1.

Table 1. List of the paired (tumor + benign) HNSCC patient samples

Serial number	**Sample**	**Location**		
		tongue	**cheek**	**gingiva**
10-T/N	tumor/benign	x		
15-T/N	tumor/benign			x
16-T/N	tumor/benign		x	
18-T/N	tumor residual/benign		x	
20-T/N	tumor/benign	x		
22-T/N	tumor/benign		x	
23-T/N	tumor/benign	x		
25-T/N	tumor/benign	x		
30-T/N	tumor/benign			x
33-T/N	tumor/benign			x
38-T/N	tumor/benign		x	
39-T/N	tumor/benign			x
40-T/N	tumor/benign			x
44-T/N	tumor/benign	x		
45-T/N	tumor suspect/benign		x	
47-T/N	tumor/benign			x
52-T/N	residual tumor/benign			x
53-T/N	tumor/benign	x		
54-T/N	tumor/benign	x		

3.3 Drug treatments and proliferation assay for the cells in 2D culture

In order to validate that Notch signaling activity was functional in the 4 cell lines selected, and required for their growth and proliferation, we tested drug efficiency on Notch activity. Two drugs, FLI 06 (cyclohexyl 1,4,5,6,7,8-hexahydro-2,7,7-trimethyl-4-(4-nitrophenyl)-5-oxo-3-quinolinecarboxylate, $C_{25}H_{30}N_2O_5$) and Yhhu 3792 (5-(3-Methoxyphenoxy)-N^2-[4-(1-methylethyl)phenyl]-2,4-quinazolinediamine hydrochloride, $C_{24}H_{24}N_4O_2$.HCl) were used to modulate Notch signaling. FLI 06 is a reported Notch pathway inhibitor, which disrupts Notch trafficking and processing (Gan et al., 2019). Yhhu 3792 has been suggested to activate Notch signaling in neural stem cells (Lu et al.,

2018). The drug efficiency was tested at 0, 0.5, 1, 3, 6, 10, 20 μM concentrations. The cells were plated into 6 well plates and the drugs were added on the next day. The protein lysates were then harvested after 24h, 48h and 72h of drug treatment and further processed with western blotting. A more detailed description about harvesting protein lysates and western blotting is described in section 3.6 and 3.8. 2D proliferation assay was performed by plating the cells on a 96-well plate (Corning) (6000 cells/well, day 0) and imaged every 2h with an IncuCyte® S3 imager device (Sartorius, Goettingen, Germany) for 4 days. The drugs were added on the next day (day 1) after the cells were plated on day 0. The proliferation curve was obtained based on phase object confluences.

3.4 The pipeline for organotypic 3D culture and quantitative analysis

In the next step, we aimed to test and validate the impact of Notch signaling activity on tumor cell growth and differentiation (organoid formation) in three-dimensional cultures. A routine experimental pipeline was established and optimized to investigate the morphological changes for the cells in 3D culture after the drug treatments (Figure 2). The ECM used in 3D culture were growth factor reduced Matrigel and Myogel (with fibrin). At first, on day 0, we seeded the cells in an Ibidi 96 well plate in Matrigel or Myogel (section 3.4.1). After that, on day 4, the drugs (FLI 06/Yhhu 3792) were added (section 3.4.2) and imaged every 2h with IncuCyte live cell imaging (section 3.4.3) for 7-10 days. For the cells grown in Myogel, the endpoint was chosen 6-7 days because cells and organoids simply grow faster, and make less defined organoids in Myogel, and therefore it was necessary to harvest or analyze them a bit earlier. While for those cells grown in Matrigel, the endpoint was a bit longer, i.e., 8-10 days. After IncuCyte live cell imaging, the cells were stained, and the plate was imaged with spinning-disc confocal microscopy (section 3.4.4) with subsequent image analysis (section 3.4.5). The details for each step are described in the following chapters.

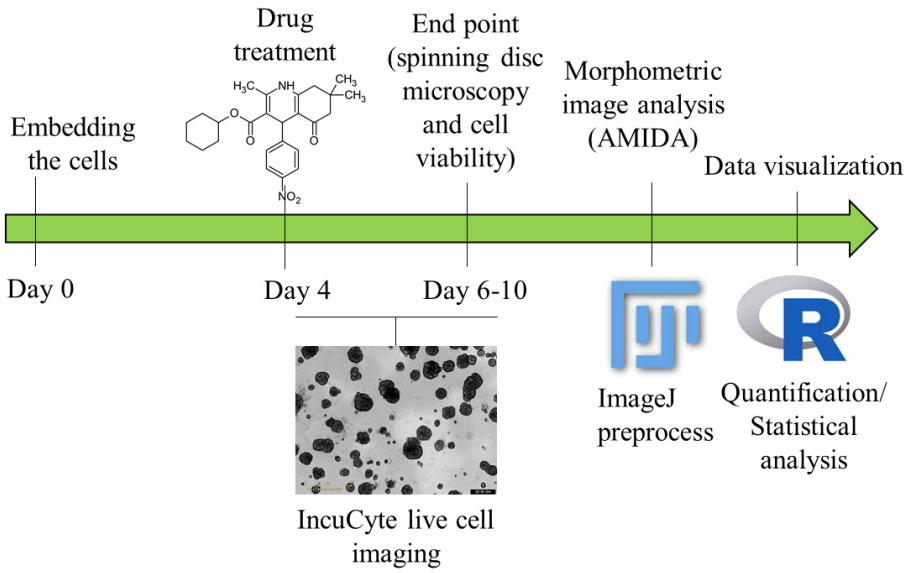

Figure 2. The optimized routine experimental pipeline for investigating the cell morphology in 3D culture after drug treatments.

3.4.1 Organotypic 3D culture

In this work, the organotypic 3D cell culture was performed as described (Härmä et al., 2014) by using uncoated angiogenesis µ-slides (Ibidi Gmbh, Germany) with the following protocol (illustrated in Figure 3): first, bottom wells were filled with 10 µl of 50% Matrigel (8 mg/ml) or 12 ul of 50% Myogel (10.9 mg/ml) (to prevent the cells from growing at the bottom of the gel) and left to polymerize at 37 ºC for 1 hour. The wells were then filled with 20 µl of cell suspension (~1000 cells/well) in 25% ECM (Matrigel or Myogel). The µ-slides were humidified by adding phosphate-buffered saline (PBS) between the wells. The upper gel consisted of 25% Matrigel or Myogel and was allowed to polymerize at + 37 ºC for 3-4h or overnight. Finally, the wells were filled with cell culture medium (ca 60 µl) which was changed every 2-3 days. The cells are brought to one focal plane by centrifugation to augment real-time imaging and automated confocal imaging at the end point of the study.

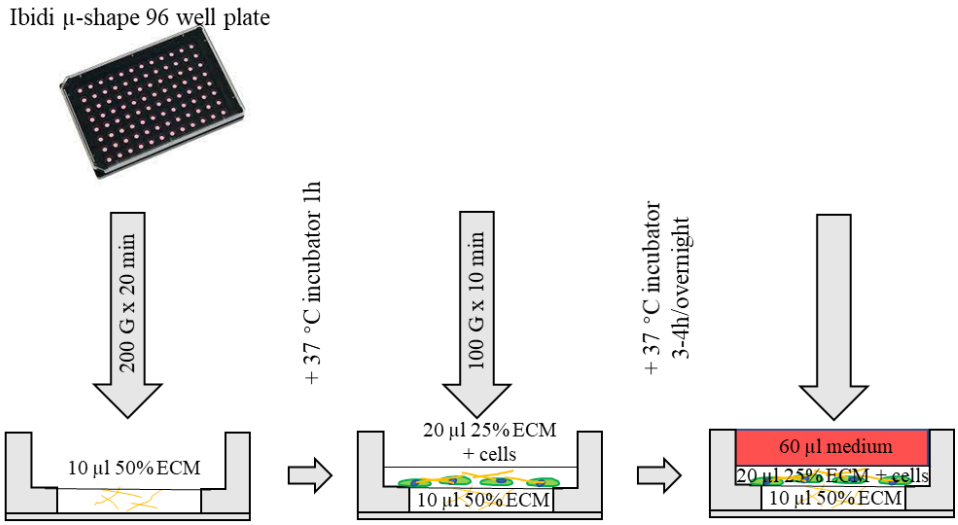

Figure 3. Ibidi Angiogenesis 96 well plate 3D cell culture protocol.

3.4.2 Notch modulation by chemical compounds

NOTCH inhibitor, FLI06, and NOTCH activator, Yhhu3792, were purchased from Tocris (Bristol, UK) and dissolved in DMSO (Dimethyl Sulfoxide). For organoids grown in 3D culture, drug treatment was initiated on day 4. The concentrations tested in this work were 0, 0.5, 1, 3, 6, 10, 20 µM for both compounds. The vehicle (DMSO) concentration was equal in all treatments, including the controls. The experiment was repeated twice with similar results and in 5 replicates in each experiment.

3.4.3 IncuCyte real-time live cell imaging

The cells in the Ibidi 96 plate were imaged with IncuCyte live cell imaging every 2h until the end point. IncuCyte living cell imaging allows us to observe the cell proliferation, morphology, and dynamic changes during the treatments.

3.4.4 Spinning disc confocal microscopy

Live cell dyes, calcein (Calcein AM), and ethidium homodimer (EthD-2), were used to stain the cells. Calcein and EthD-2 were mixed with the medium 1: 1000 and added to the cells in 3D plates and incubated at 37 °C for 1h, and subsequently measured with a Zeiss Axiovert-200M microscope, equipped with Yokogawa CSU22 spinning disc confocal unit using Zeiss Plan-Neofluar 5x objective confocal microscopy. EthD-2 is a membrane-impermeable fluorescent dye for living cells but is able to enter disrupted membranes, upon which it enters the nucleus and binds to DNA of dead and dying cells. EthD-2 is maximally excited by light with a wavelength of ~535 nm and emits red fluorescence with an emission maximum of ~624 nm. Calcein AM (Thermo Fisher) is a cell-permeant dye used to stain the living cells and visualize the morphologies of multicellular 3D spheroids. In live cells, after acetoxymethyl ester hydrolysis by intracellular esterases, the nonfluorescent Calcein AM is converted to a green, fluorescent calcein which emits green fluorescence with an emission maximum of ~520 nm. The light wavelength used to excite Calcein AM stained cells was 488 nm.

3.4.5 Quantitative phenotypic analysis with AMIDA

Quantitative phenotypic analysis was carried out by using the automated image analysis software, AMIDA, described in section 1.6. AMIDA was originally designed for retrieving information from 3D confocal image stacks (Härmä et al., 2014). To facilitate the streamline analysis, the stacks of 3D images taken by the confocal microscope were first converted to 2D images with maximum intensity projections. After that, several representative 2D images were tested with AMIDA to define the optimal settings (threshold, sensitivity) for subsequent image segmentation (based on watershed segmentation method) to be used in batch analysis mode. The ideal "sensitivity" used in AMIDA analyses refers to the distance in pixels and controls the effective splitting of segmented cell regions by water-shedding. A smaller sensitivity value is typically more sensitive and leads to smaller (but also more) segmented regions. The "threshold" value used in AMIDA settings determines the cut-off value of the histogram. That is, all the values/pixels below the threshold value will be excluded or filtered out. Once the optimal settings for batch image analyses were determined, these were retained for segmentation

of all the images from the same experiment, obtained during the batch analysis. For batch analysis, the sensitivity in this work was set 10-20 and the threshold value was 1, the smallest value was 150-300 (pixels). For each image, AMIDA extract individual multicellular structures and assigns simultaneously the corresponding numerical values to the objects. A representative 2D maximum intensity projected image from HNSCC cells grown in Matrigel in 3D culture before and after segmentation is shown in Figure 4. Table 2 is the list of the parameters selected for quantitative analysis of the phenotypic changes in organotypic 3D culture. AMIDA offers many more morphometric parameters, which were not used in this analysis. "Area" illustrates the size of the object, measured in pixels, while "Roundness" indicates the symmetry of the organoids in % of perfect round shape.

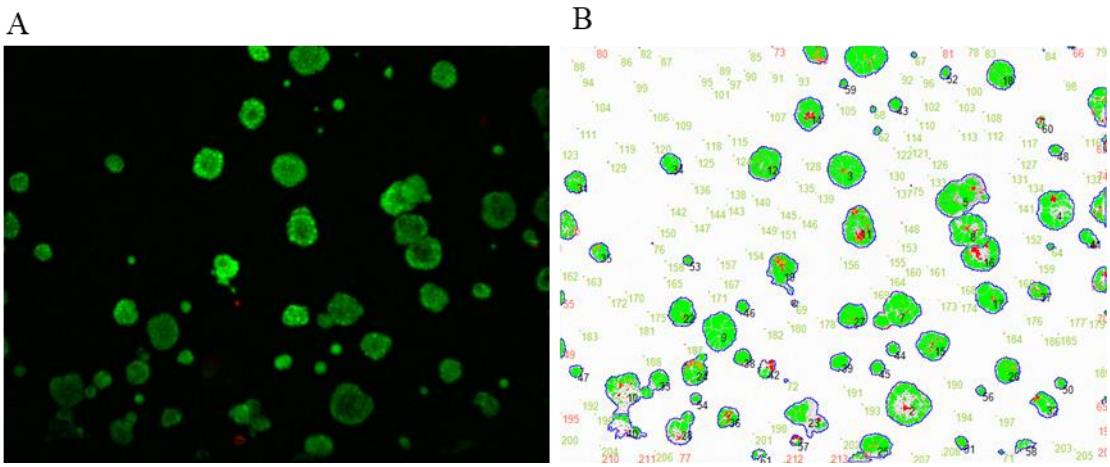

Figure 4. A representative 2D images obtained from 3D images with maximum intensity projection before (A) and after (B) segmentation. The objects marked in blue circle are analyzed, while all the objects marked in red or green are excluded.

Table 2. Description of AMIDA parameters used in this study

Parameter	Description
Area	Area of the segmented structure (in pixels)
Roundness	Roundness of the segmented structure (in percentages)

3.5 Cell metabolic viability assay

The cell viability assay for the cells cultured in 2D or organotypic 3D culture was performed by using a colorimetric detection method with Cell Counting Kit-8 (WST-8/CCK8, DojinDO Laboratories, Japan) mixed with the medium in 1:10. The mixture was added to the cells and incubated at 37 ºC for 45 min - 1 h. During incubation, the water-soluble tetrazolium salt in WST-8 was reduced by cellular dehydrogenases to a medium-soluble orange formazan product. The amount of formazan produced is directly proportional to the number of living cells and was measured by absorbance at 450 nm with a plate reader (WALLAC VICTOR^2).

3.6 Harvest protein lysates from cultured cells

To study the expression of NOTCH in the UT-SCC cell lines. The cells from each cell line were cultured on one well in a 6 well plate (Corning) with a cell density of 200,000 cells/well and harvested with 100 µl of lysis buffer (plus phosphatase and proteinase inhibitors) after ~72h when the cells were nearly confluent. Three biological samples from each cell line were collected.

To study the drug effects on NOTCH expression, the cells from UT-SCC-42A cell line were cultured on a 6 well plate with a cell density of 300,000 cells/well as shown in Figure 5. The drug was added the next day after the cells were plated. The protein lysates were harvested with 60/70 µl of lysis buffer after 24h, 48h and 72h. Three biological replicates were collected.

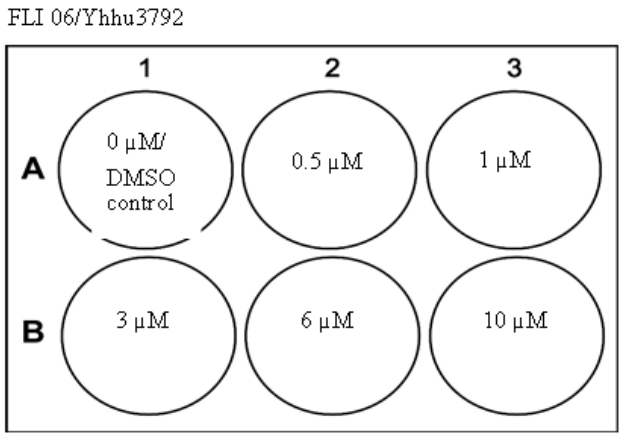

Figure 5. The 6 well plate map for the cells with the drug (FLI 06 or Yhhu3792) treatments.

In terms of the siRNA transfected cells, cells were plated in a 12 well plate (Corning) and harvested with 40/60 µl of lysis buffer per well accordingly, based on the transfection protocol (see section 3.10).

When harvesting protein lysates, the plates were kept on ice to inhibit cellular activity and proteolysis. The cells were washed once with 1 ml of cold PBS and scraped off the plastic surface with a single-use scraper. After that, the protein lysates were put on ice and mixed a couple of times for 20 min, centrifuged for 10 min at 4 ºC, and stored at -20/70 ºC for further use. The recipe of the lysis buffer-base is shown in Table 3. The phosphatase (Pierce™ Protease Inhibitor Mini Tablets, EDTA-free) and proteinase inhibitors (Pierce™ Phosphatase Inhibitor Mini Tablets) were added to an aliquot of lysis buffer-base before use or stored as aliquots in -20 ºC.

Table 3. Recipe for lysis buffer-base

175.6 ml	Milli-Q water
2 ml	Triton x100 (1%) (or NP-40)
4 ml	1 M TrisCl pH 7.5 (20 mM)
400 µl	0.5 M EDTA (1 mM)
4 ml	0.5 M NaF (10 mM) (phosphatase inhibitor)
4 ml	5 M NaCl (100 mM)

3.7 RNA isolation from patient samples and cultured cell lines

The RNA lysates for the cultured cell lines were harvested at the same time when harvesting the protein lysates from the same plate but different wells. The RNA lysates were harvested with 350 µl of buffer RLT plus per well (Qiagen, Hilden, Germany), and three biological replicates were collected. The total RNA isolation was done with miRNeasy Tissue/Cells Advance Mini Kit (Qiagen) according to manufacturer's protocol.

For the HNSCC patient samples received from the clinics, the RNA lysates were obtained by disrupting the tumor or normal tissues in 600 µl of lysis buffer using an ULTRA-TURRAX homogenizer. After disruption, the lysates were vortexed for 30 seconds and centrifuged at full speed for 3 min. The supernatants (total RNA extraction) were then processed with RNeasy® Plus Mini Kit (Qiagen) according to manufacturer's protocol. To avoid RNA degradation, the biopsies were kept in between dry ices before disruption.

The RNA concentrations and purity values for the cell lines and patient biopsies were measured by NanoDrop One (Thermo scientific).

3.8 Western blotting

In this work, the protein expression levels in cell lysates were studied by western blot. First, the protein lysates harvested from the cells were quantitated by using Pierce™ Bicinchoninic Acid (BCA) PROTEIN Assay Kit (Thermo scientific) according to the manufacturer's protocol. The protein concentration was analysed using a spectrophotometer (PerkinElmer/WALLAC VICTOR^2) to measure the absorbances at 600 nm and determined based on BCA standards. Before concentration analysis, the protein samples were centrifuged at + 4 ºC for 5 min and the supernatants were diluted with lysis buffer 1:2 or 1:4 which was taken into account in protein concentration calculations.

Based on the concentration measurements, equal amounts of protein were taken from each sample and prepared for SDS-page and western blotting. The protein samples were first heated at 95 ºC for 5 min for denaturation. After that, the samples were separated on a 4-15% mini-PROTEAN TGX precast gel (Bio-Rad, USA) and transferred to Nitrocellulose Pure Transfer Membrane (Santa Cruz Biotechnology Ltd). The membranes were dried between two blotting papers overnight, and re-wetted with Milli-Q water the next day. The membranes were then blocked with 5% non-fat milk in TBS-Tween buffer for 30 min at room temperature and incubated with primary antibodies overnight or during the weekend at 4 ºC. After washing with TBS-Tween three times, the membranes were incubated with the secondary antibody in 5% non-fat milk solution for 1 hour at room temperature. The membranes were then imaged with Li-COR Odyssey Infrared Imaging System to evaluate the protein expression. The stripping of the membrane was done by using in-house stripping buffer/commercial stripping buffer. The primary and secondary antibodies used in this study are listed in Section 3.4. The quantification/densitometry analysis of western blot bands was carried out with the Image studio lite software (Li-COR Biosciences).

3.9 Primary and secondary antibodies

For western blotting, the primary antibodies used in this study were: PSMD2 rabbit (ab140675), HES5 (EPR15578) rabbit, NOTCH1 ((D1E11) XP(R)) rabbit mAb, NOTCH2 (D76A6) rabbit mAb, NOTCH3 (D11B8) rabbit mAb, HES1 (D6P2U) rabbit, Jagged1 ((D4Y1R) XPCR) rabbit mAb, DVL3 rabbit Ab, p44/42 MAPK (Erk1/2) rabbit Ab and P-p44/42 MAPK (T202/Y204) rabbit Ab. Except HES5 and PSMD2 were purchased from Abcam, Cambrige, MA, USA, all other primary antibodies were purchased from Cell Signaling Technology, Beverly, MA, USA. β actin (C4) mouse monoclonal IgG_1 (Santa Cruz Biotechnology) was used as house-keeping gene. The secondary antibodies used were anti-rabbit-IR800 (Li-Cor Biosciences, Lincoln, NE) and anti-mouse IgG (H+L) (DyLight^{TM} 680 conjugate) (Cell Signaling Technology).

3.10 DVL3 and PSMD2 silencing with siRNA transfection

siRNA transfection of DVL3 or PSMD2 in UT-SCC-42A cells was performed using Lipofectamine RNAiMAX (Invitrogen, Canada) according to the reverse transfection method. For siRNA optimization, 2 µl of RNAiMAX reagent was diluted in 100 µl of Opti-MEM (Life Technologies Limited, UK), and 0.5, 1, 2 µl of siRNA (5 µM stock) was diluted in Opti-MEM® reduced serum medium to achieve the final siRNA concentration of 2.5, 5 and 10 nM, respectively. The RNAiMAX and siRNA diluted solutions were combined and transferred to a 12 well plate (Corning) and incubated for 15-20 min at room temperature. 0.8 ml of UT-SCC 42A cells in antibiotics-free medium (10% FBS, DMEM (Gibco™/Invitrogen), antibiotics-free) were plated on top of the reagent mixture (150,000 cells/well). After 48h, protein lysates were harvested, extracted, and analyzed by western blotting.

After optimization, to study the effect of DVL3 knock down on cell growth and viability in 3D culture, the two most effective siRNAs with optimal concentrations were selected for siRNA transfection using the same reverse transfection method. The cells were first plated into a 12 well plate (Corning) in three replicates (wells) for controls and transfected (Figure 6). After 24h, the cells were trypsinized from two wells for each condition and seeded into two ibidi 96 well plates in either MTG or MYO, respectively. The cell density was 1000 cells/well and the plates were imaged every day with IncuCyte live cell imaging. At the end point of the study, the plates were imaged by spinning disc confocal microscopy, followed up with the WST8 metabolic viability assay. The rest of cells were plated into new 12 well plates and the protein lysates were harvested after 48h to monitor the gene knock-down after trypsinization. In addition, the protein lysates were harvested from the cells left in the original plates (wells on lines C, Figure 6) after 48h of culture and further processed for western blotting. A simplified workflow for the (DVL3 siRNA) transfection experiments is shown in Figure 6.

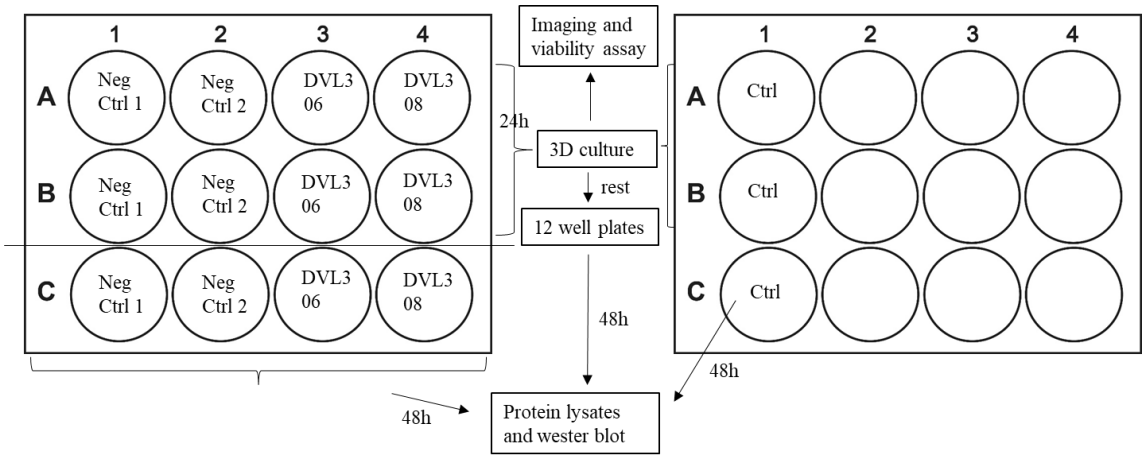

Figure 6. A simplified workflow for DVL3 siRNA transfection experiment.

The siRNAs used in this work are Dharmacon^{TM} ON-TARGETplus siRNA Human PSMD2 (Cat#: J-017212-06-0005, J-017212-07-0005, J-017212-08-0005, J-017212-08-0005) and Human DVL3 (Cat#: J-004070-05-0005, J-004070-06-0005, J-004070-07-0005, J-004070-08-0005). Ambion Negative Control siRNA #2 (Ambion) and AllStars Negative Control siRNA (Qiagen) were used as negative controls.

3.11 Quantitative real-time PCR (qPCR)

For real-time qPCR, 1 µg of total RNA was first reverse transcribed into complementary DNA (cDNA) with Maxima reverse transcriptase (Thermo Scientific) and Oligo d(T)18 primer (NEW ENGLAND BioLabs$_{INC}$). Real-time qPCR was performed using 2x DyNAmo HS SYBR Green qPCR Master Mix (Thermo Scientific, Vilnius, Lithuania) with a Bio-Rad CFX384^{TM} real-time PCR detection systems. The primers for amplification of DVL3 (F: 5'-TGG ACG ACG ATT TCG GAG TG-3', R: 5'-CTG TTC TGT GGA GCT GCT GA-3') and PSMD2 (F: 5'-ATG GGG TCA TGA GTA TGT CAG G-3', R: 5'-CTG CAC TCA ACA TTC CGT GG-3') were designed based on NCBI databases (http://www.ncbi.nlm.nih.gov/ tools/primer-blast/). One primer for amplification of PSMD2 (F: 5'-ACT GGA GGT TGT GTC AGA GC-3', R: 5'-GTT CGC TAC AAA TGT GGA GCA GC-3' was bought from OriGene as comparison. The sequences for NOTCH3 primers are F: 5'-GCAGATGGCTCAACGGCACTG-3', R: 5'-GGGGTCTCCTCCTTGCTATCCTG-3' (synthesized by Genomed company). The total

mRNA of gene of interest was quantified by absolute quantification method and normalized to GAPDH (F: 5'-TCC TGT TCG ACA GTC AGC CG-3', R: 5'-CCC CAT GGT GTC TGA GCG AT-3').

3.12 Statistical analysis

For biological and experimental replicates, data are shown in mean with standard deviations (s.d.). In AMDIA analysis, the statistic significant difference in object size (area) and symmetry (roundness) between the drug treated and control is assessed by multiple-sample corrected *t*-test against control. $p < 0.05$ is considered as significant different. To compare the significant difference for the expression of DVL3 and PSMD2 in patient normal and tumor tissues, Shapiro-Wilk test was first performed to detect the normality among normal and tumor groups. For data with normal distribution, 2-tailed student's T test was performed. For data which were not normally distributed, Wilcoxon signed-rank test was performed. $P < 0.05$ is considered as significant different.

4. RESULTS

4.1 Analysis of Notch signaling in the cell lines

As seen from the western blot results (Figure 7), both Notch receptors (NOTCH1-3) and one of the Notch ligands (JAG1), as well as two Notch targeted genes (HES1, HES5) are all expressed in the studied four cell lines. Especially, the expression of cleaved NOTCH (NTM NOTCH1-3) receptors and the target genes indicate that NOTCH is activated and active in these cells, respectively. It appears that NOTCH1, NOTCH3 and HES5 are expressed at higher levels (stronger signals at 120, 90, 18 kDa) in UT-SCC-24A and B compared to 42A and B. There was no significant difference for NOTCH2, HES1, JAG1 expression across all cell lines. In addition, NOTCH3 primary antibody recognized also some other non-specific bands (multiple size of bands near FL and NTM). Therefore, qPCR was further performed to verify this. In agreement with the western blot results, NOTCH3 expression was lower in UT-SCC-42 than in UT-SCC-24 cell lines, also at the mRNA level (Appendix I).

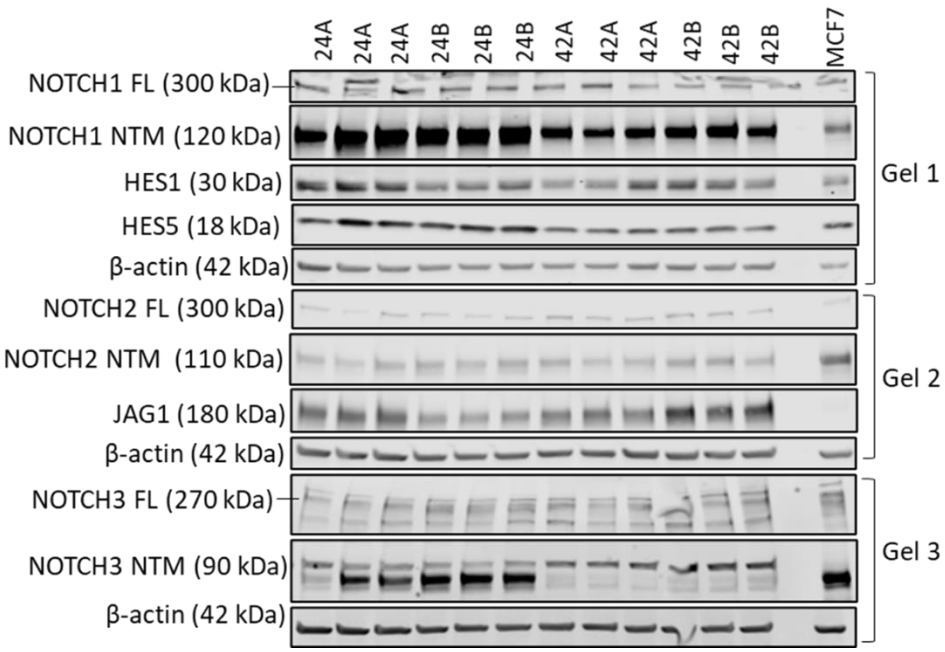

Figure 7. NOTCH expression in the UT-SCC cell lines. Western blot analysis. The western blotting was made on three SDS gels to avoid the overlapping of the signals from NOTCH1, NOTCH2 and NOTCH3. NTM is the N-terminal and intracellular part of NOTCH, meaning cleaved NOTCH that enters the cytoplasm and nucleus. FL (full length) refers to the complete, noncleaved form of NOTCH receptors that is membrane-associated and represent the inactive form of NOTCH. NOTCH (NOTCH1-3), Jagged ligand (JAG1) and NOTCH targeted genes (HES1, HES5) are all expressed in the studied cell lines. n = 3.

4.2 Functional role of Notch signaling in cancer cell growth and viability in 2D and 3D cultures

From section 4.1, we have validated that Notch is active in our studied models, next, we are interested to know what its functional role in these cell lines is. First, we tested the drug efficiency on Notch activity. In this case, the Notch inhibitor FLI 06 and the Notch activator Yhhu 3792 were examined to verify their function as inhibitor/activator of the overall Notch signaling activity and NOTCH cleavage at molecular level. This was done by looking at the gene expression at protein level using western blots. The western blot results and the effect of drug treatments on UT-SCC 42A proliferation, metabolic viability, and phenotypes in 2D and 3D culture will be described in the following sections.

4.2.1 The effect of FLI 06 on Notch activity and HNSCC cell function

Figure 8 shows the western blots results for the FLI 06 treated cells. As seen from the figure, NOTCH1 activation was reduced by FLI06 at higher concentrations (6 and 10 µM). This was observed by an increase in FL- and decrease in NTM (cleaved)-NOTCH1 expression on the blots. In addition, the expression level of cleaved and full length NOTCH3, HES1 as well as HES5 was decreased with 6 and 10 µM of FLI 06 which indicates that the Notch signaling activity was also supressed.

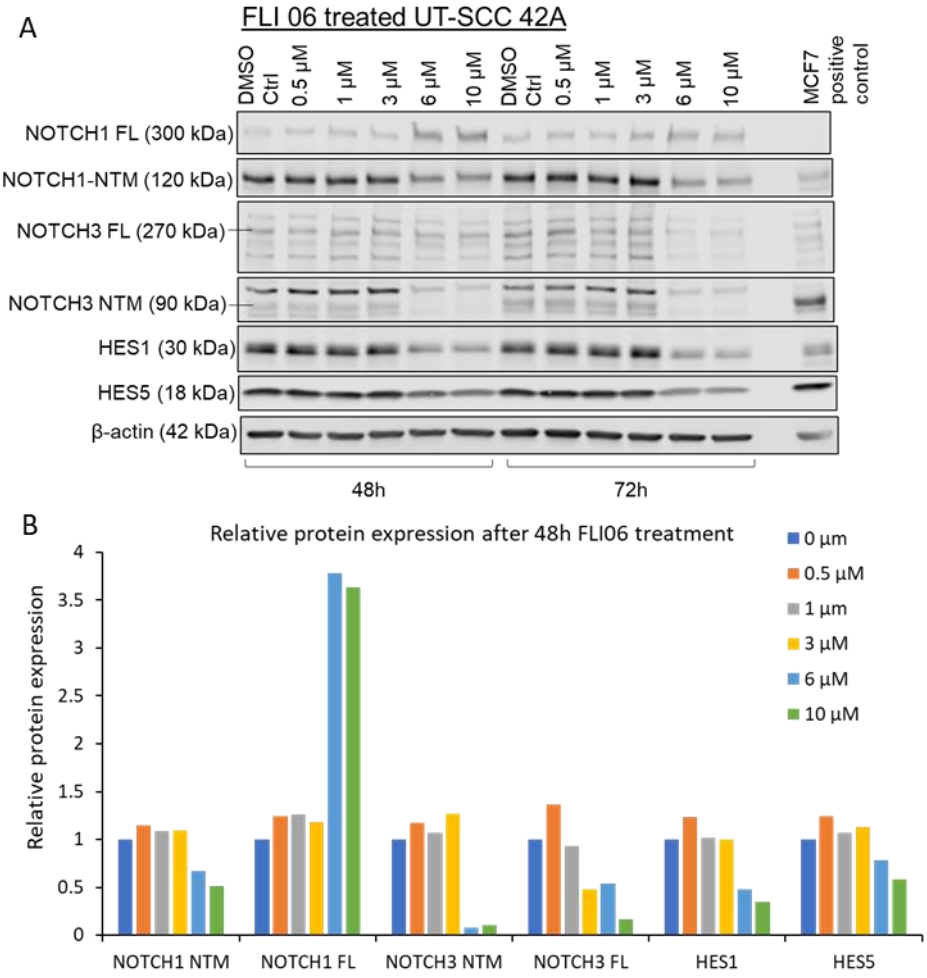

Figure 8. FLI 06 inhibited Notch activation and activity. A) Images showing expression of NOTCH1, NOTCH3, HES1 and HES5 after 48 and 72h treatment. B) Quantification of the blots (48h) with densitometry and image studio lite. Proteins extracted from MCF-7 cell line is used as a possible reference, and comparison to previous experiments with breast cancer cell lines.

In addition, it was found that for the cells grown in 2D culture, FLI 06 reduced cell proliferation, viability and caused phenotypic changes over the concentration, especially at higher concentrations (3, 6, 10 µM) (Figure 9). The inhibition of cell proliferation started ~24h after drug was added (Figure 9B) and the cells appeared more rounded than the original elongated structures observed in untreated cultures (Figure 9A). After performing the real-time proliferation assay with the IncuCyte imager, the cell viability was measured on day 4 (after 72h of drug treatment). The results shown in Figure 9C indicate that the cell viability decreased with increasing of FLI 06 concentration. Simultaneously, the dramatic morphologic changes started to be visible from a concentration of 3 µM (Figure 9A). The morphological changes for FLI 06 treated cells at 3, 6 and 10 µM were observed already on day 2/after 24h of starting the treatments (Appendix II).

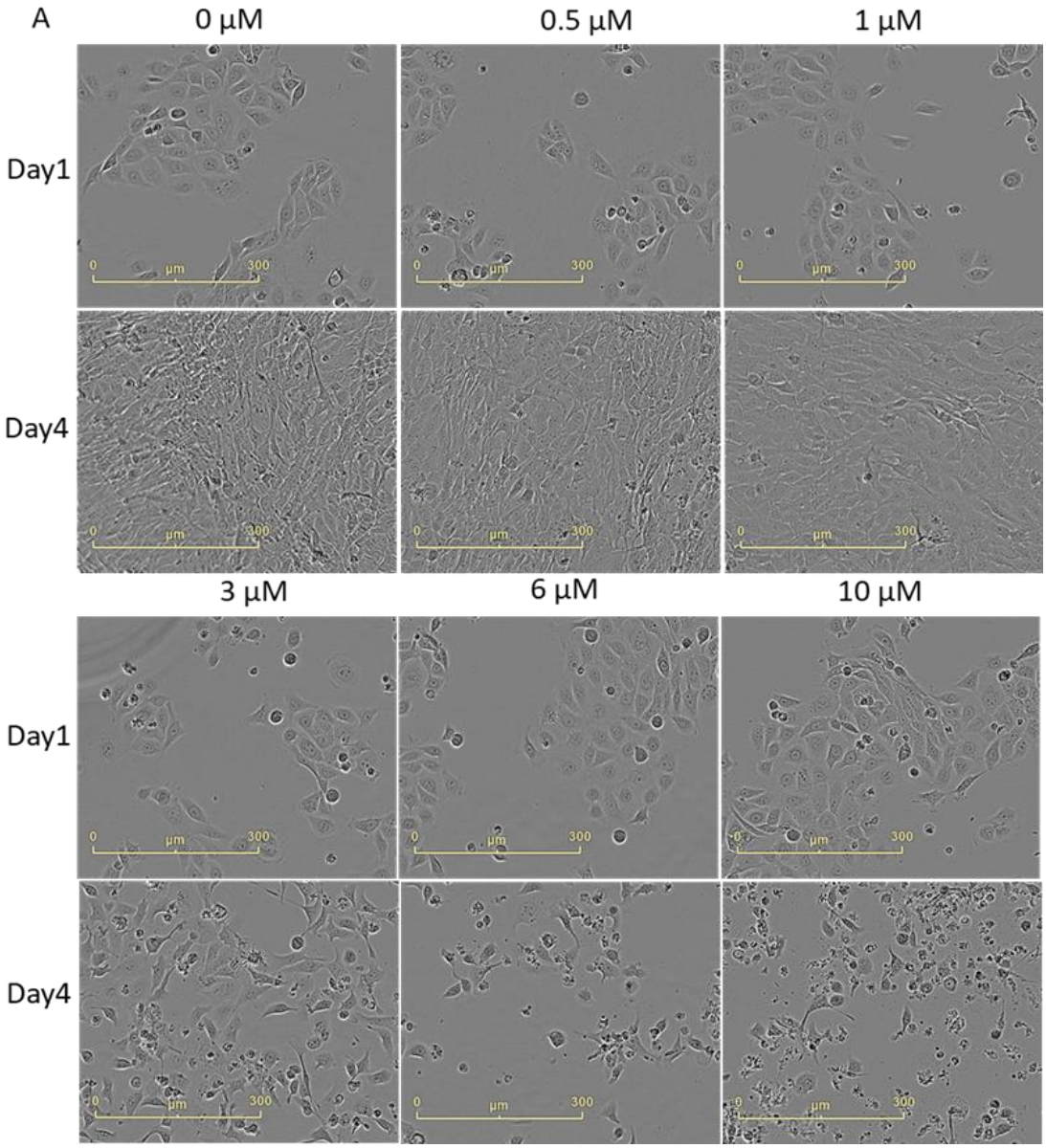

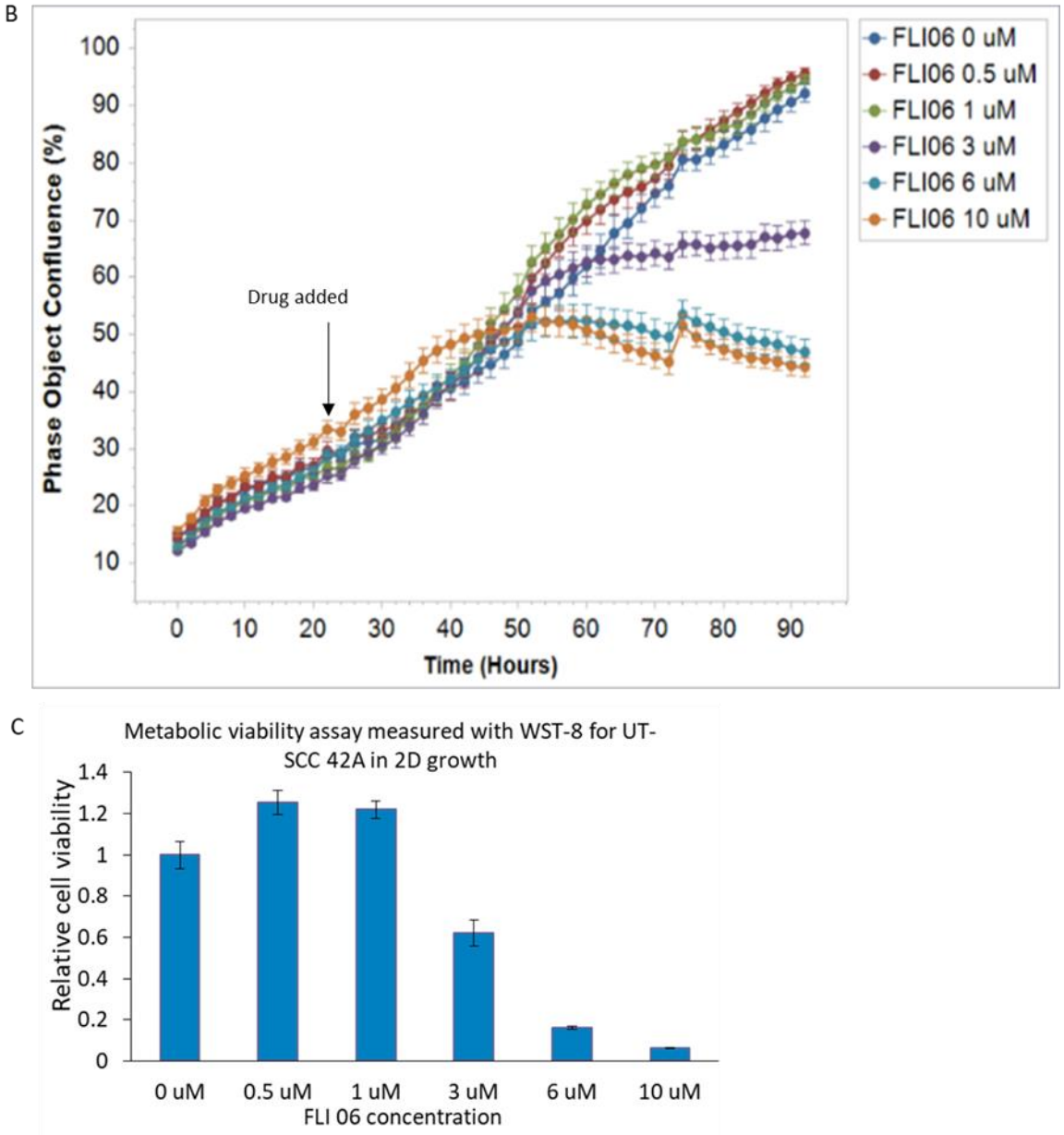

Figure 9. Effects of FLI 06 on cell growth and viability in 2D culture. A) Representative live cell images of FLI 06 treated cells in 2D culture, measured by IncuCyte. Drug was added on day 1 (the next day after the cell was plated). The images shown here were captured before the drug was added (marked as Day 1 in the images), and after 72h (marked as Day 4) of drug treatments. For the control treatments (0 µM), DMSO was added as vehicle control. The magnification is 10x. B) Proliferation curve (cell culture confluence) of UT-SCC-42A treated with FLI 06. Number of replicated wells is 5. C) Relative metabolic viability (measured on day 4) for the control and FLI 06 treated cells grown in 2D culture. Data presented as mean ± s.d. n = 5.

Regarding to the cells in 3D culture, the cells were found growing differently in Matrigel (Figure 10A) compared to Myogel (Figure 11A). In Matrigel, cells grew as more or less rounded organoids, while in Myogel, the cells appeared more invasive, and "organoids" were more spindle-like and generally showed more complex multicellular structures. From Figure 10, we can see that the cell morphology, proliferation, and viability in Matrigel is concentration dependent. The organoids formed in Matrigel became smaller (Figure 10A, B and C) and the invasiveness (spindle-like structures) of the "organoids" in Myogel was inhibited over the drug concentration. (Figure 11A and B). The cell morphology in Matrigel was also significantly reduced over the concentration, especially at 3, 10, and 20 μM (Figure 10D). In addition, some apoptosis was likely occurred in Myogel at higher drug concentrations (10 and 20 μM). The metabolic viability of cells in Myogel was not measured since part of the cells started to grow at the bottom of the plates as monolayers after 3 days of drug treatments and thus would not represent the 3D properties.

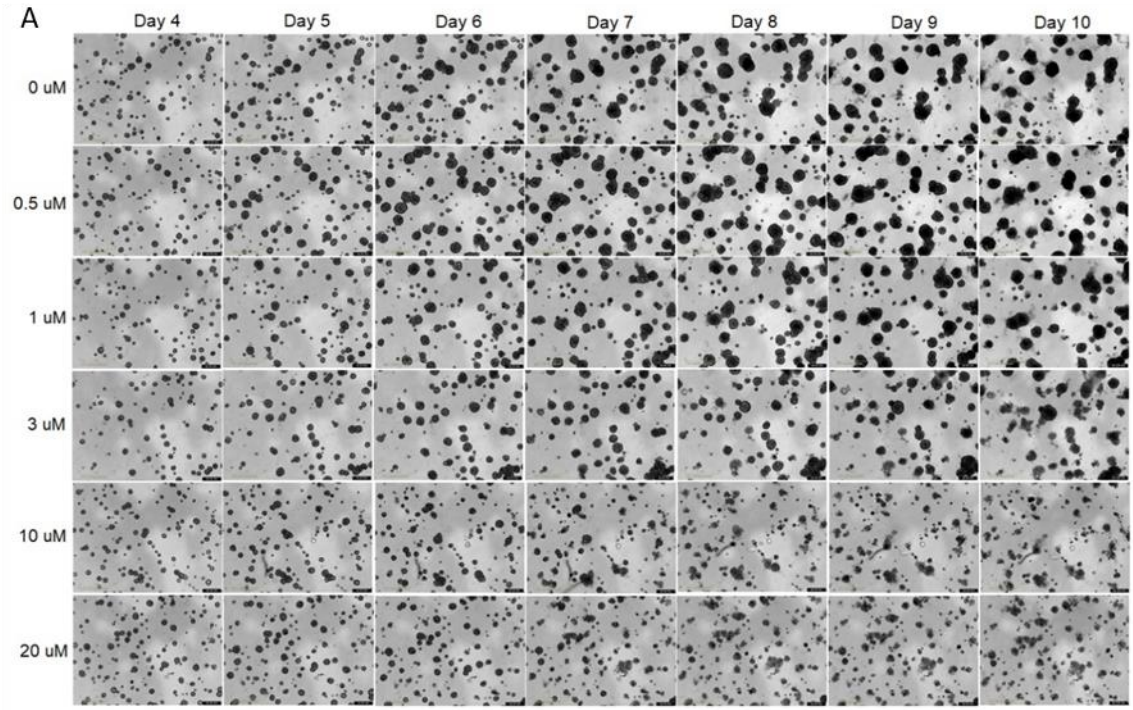

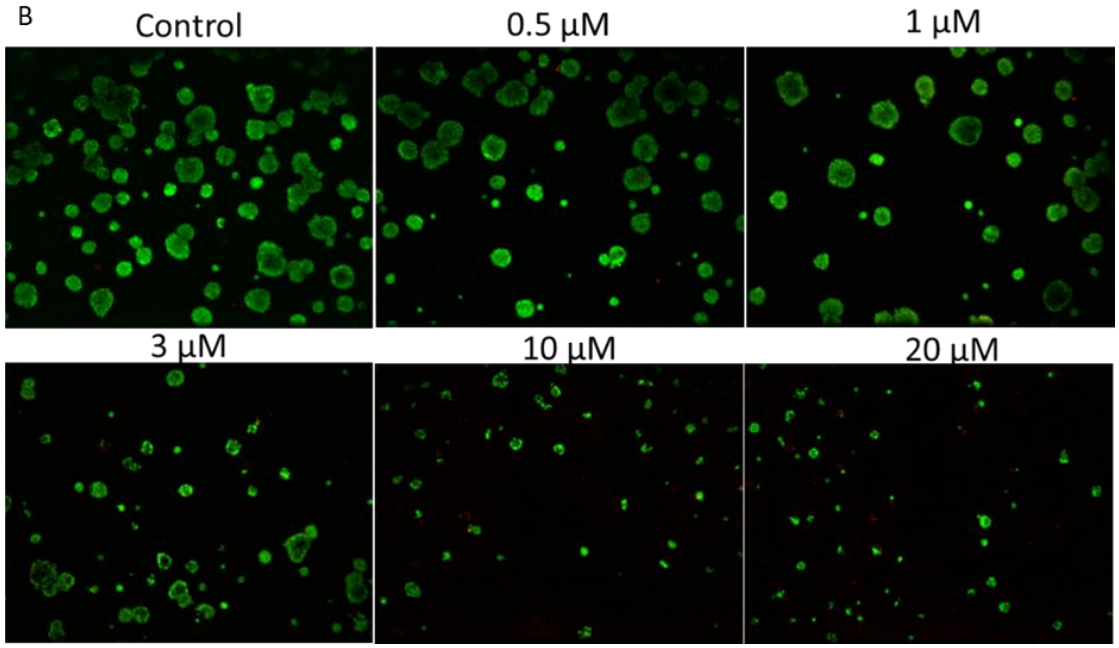
B
Control
0.5 µM
1 µM
3 µM
10 µM
20 µM

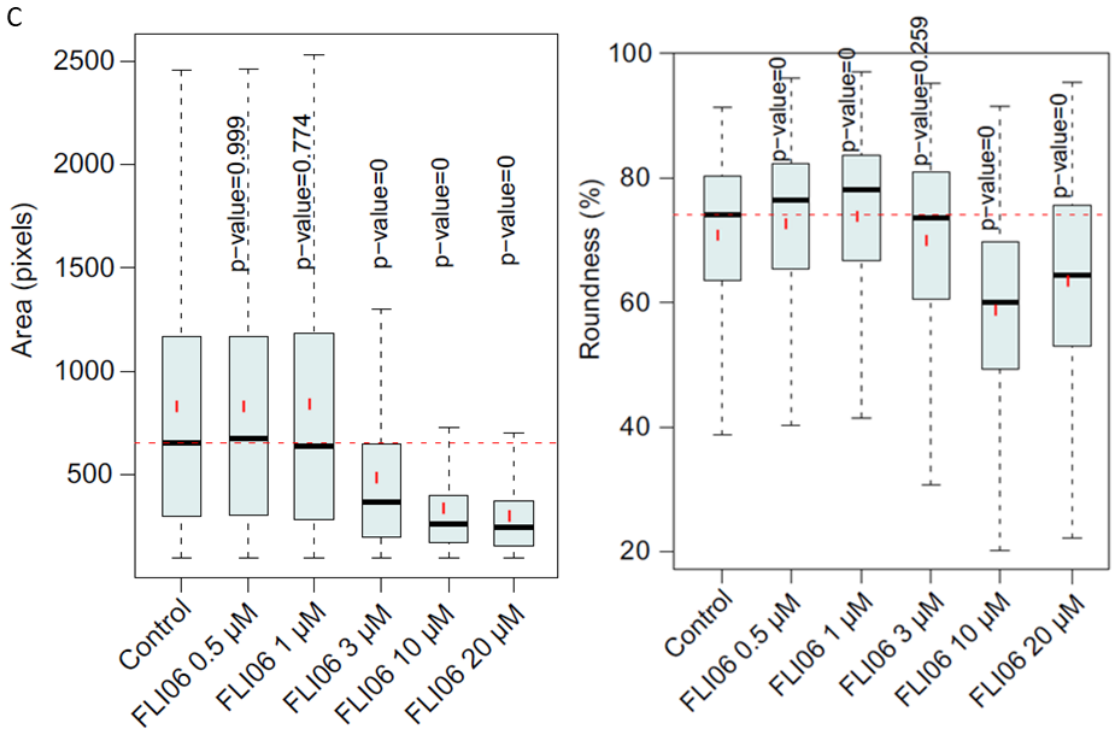
C
Area (pixels)
2500
2000
1500
1000
500
p−value=0.999
p−value=0.774
p−value=0
p−value=0
p−value=0
Control
FLI06 0.5 µM
FLI06 1 µM
FLI06 3 µM
FLI06 10 µM
FLI06 20 µM
Roundness (%)
100
80
60
40
20
p−value=0
p−value=0
p−value=0.259
p−value=0
p−value=0
Control
FLI06 0.5 µM
FLI06 1 µM
FLI06 3 µM
FLI06 10 µM
FLI06 20 µM

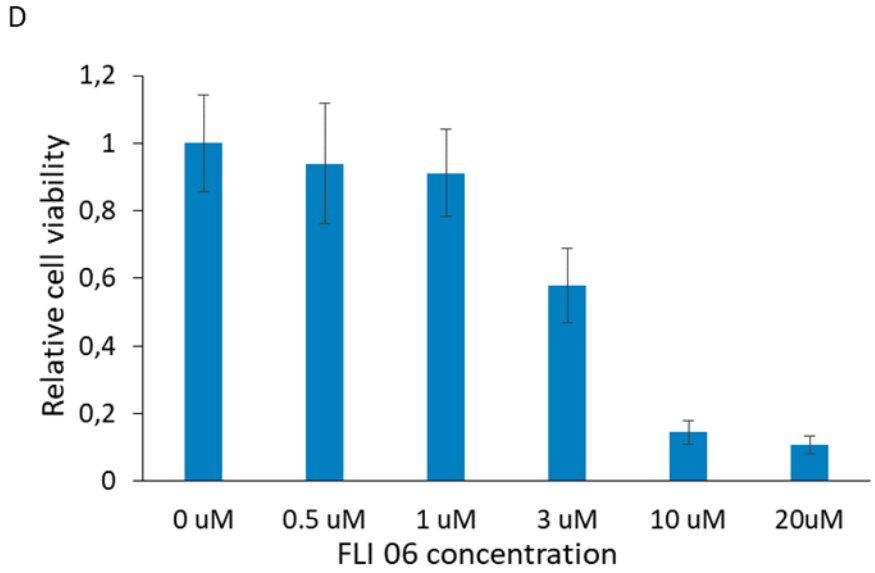

Figure 10. Effect of FLI 06 on cell growth, viability, and phenotypic changes in Matrigel in 3D culture. A) Representative live cell images show the cell growth in Matrigel at different drug concentrations and timepoints. Cells were seeded on day 0, drug was added on day 4. Microscopic images shown were taken before drug was added (marked as Day 4) and every 24h after adding the drug for a period of 6 days. For control treatments, DMSO was added as vehicle control. The magnification used is 10 x. B) Confocal images of Calcein AM (green) and EthD-2 (red) stained organoids. Images were captured on day 10. The magnification is 5 x. C) Quantitative image analysis for FLI 06 treated UT-SCC 42A in Matrigel in 3D culture by AMIDA. n = 5. Boxplots show the difference between the drug-treated and control for the selected features (i.e., area, roundness). Black bar is median, red dot is mean. The statistics that AMIDA plots show are multiple-sample corrected t-test against control. $p < 0.05$ is considered as significant different. D) Cell metabolic viability in Matrigel in 3D culture (measured on day 10). n = 5.

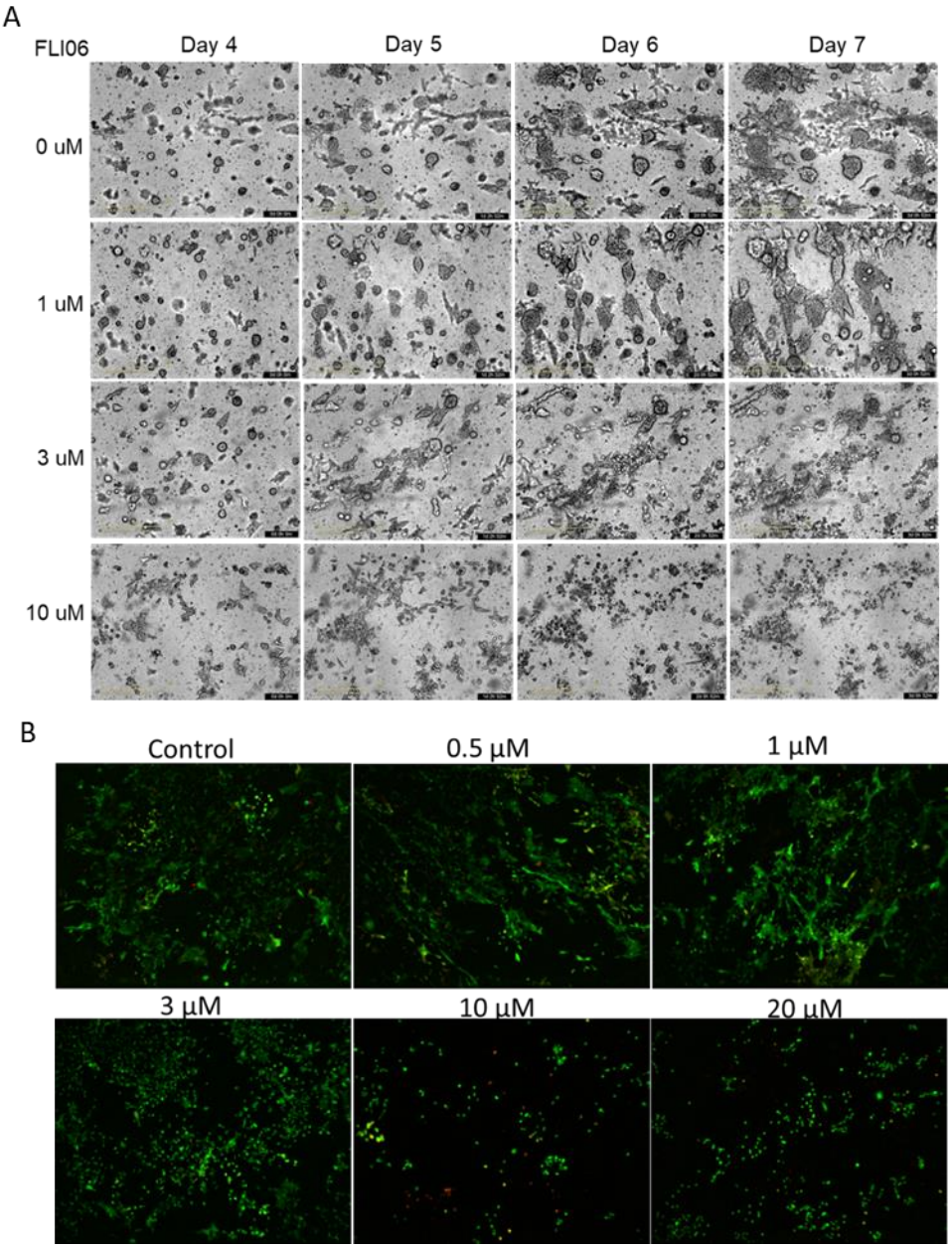

Figure 11. Effect of FLI 06 on cell growth, viability, and phenotypic changes for UT-SCC-42A in Myogel in 3D culture. A) Representative live cell images of FLI 06 treated cells embedded in Myogel, as measured by IncuCyte. Cells were embedded on day 0. Drug was added on day 4. The representative images shown were taken before drug was added (day 4), and after 24h (day 5), 48h (day 6), and 72h (day 7) of drug treatments. For control experiments, DMSO was added as vehicle control. The magnification is 10 x. B) Confocal images of Calcein AM (green) and EthD-2 (red) stained organoids. Images were captured on day 7. The magnification is 5 x.

4.2.2 The effect of Yhhu 3792 on Notch activity and HNSCC cell function

Yhhu 3792 has been reported to activate the Notch signaling in neuronal stem cells. However, in our study, as seen from the western blot results (Figure 12), no significant increase on the expression level of NOTCH and NOTCH targeted proteins was observed with the chosen drug concentrations and timepoints. Instead, based on the quantification results (Appendix III), the expression at least of activated NOTCH3 protein (NTM) was slightly decreased, corresponding to an increase in expression of full length NOTCH3 and a slight decrease in HES1, also likely in HES5 expression after 48h treatment with 3, 6, 10 μM of Yhhu 3792. In other words, this drug, which was supposed to activate the Notch signaling pathway may have the opposite effect.

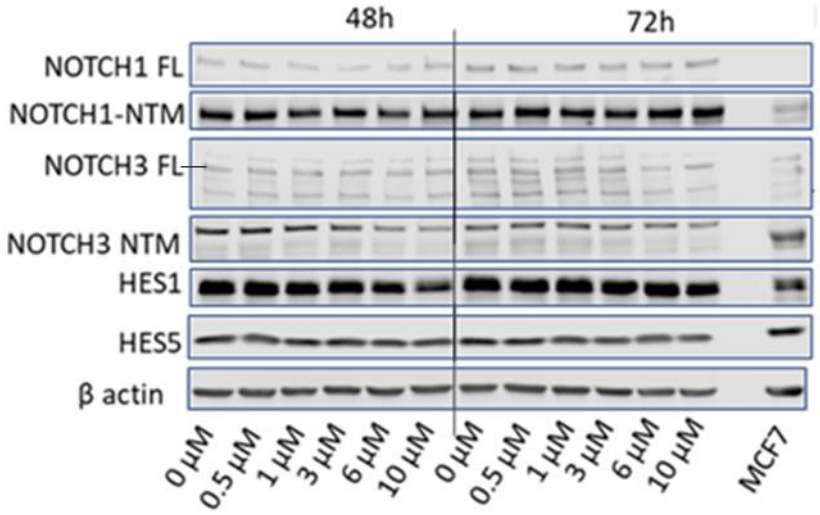

Figure 12. Effect of Yhhu 3792 on NOTCH activity. Western blot showing NOTCH1, NOTCH3, HES1 and HES5 protein expression in UT-SCC 42A, treated with Yhhu 3792 after 48 and 72h. Proteins extracted from MCF-7 cell line is used as a possible reference, and comparison to previous experiments with breast cancer cell lines.

Despite the failure to clearly show Notch activation, Yhhu 3792 was still used to treat UT-SCC-42A cells to see its functional effects. For the cells in 2D culture, the live cell images (Figure 13A) indicate that no morphological sign of cytotoxicity was observed for Yhhu 3792 treated cells (Appendix IV). At higher Yhhu 3792 concentration (3, 6, 10 μM), cell proliferation was slightly decreased. However, the overall cell viability was increased, especially with 6 and 10 μM drug treatment.

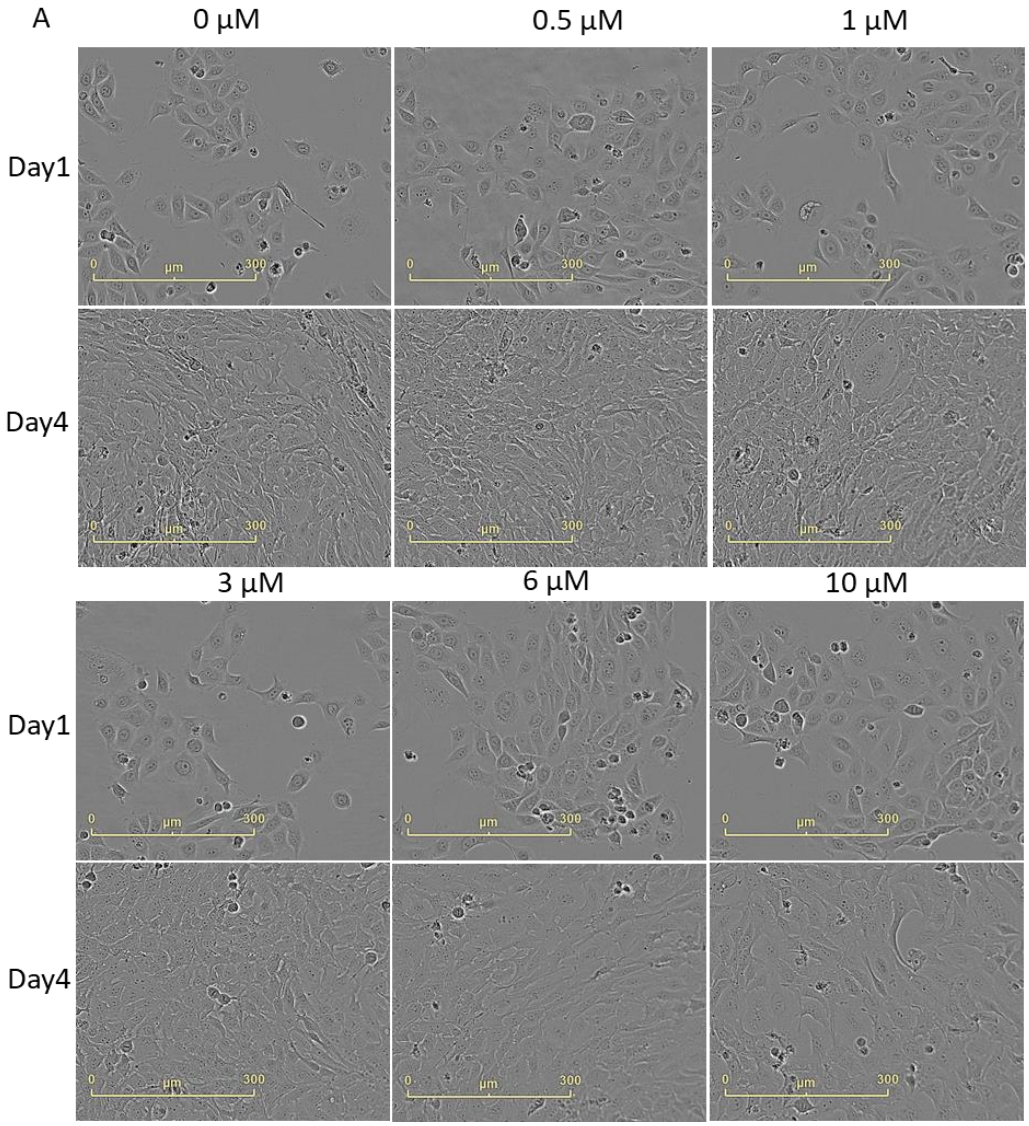
A
0 µM
0.5 µM
1 µM
Day1
Day4
3 µM
6 µM
10 µM
Day1
Day4

B

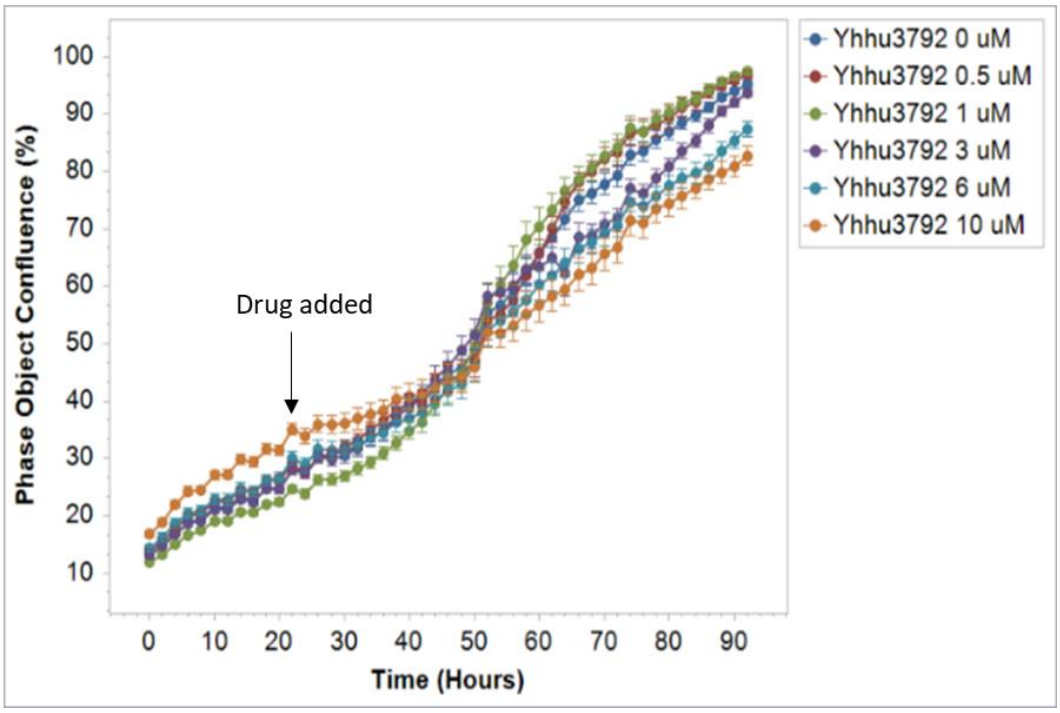

C

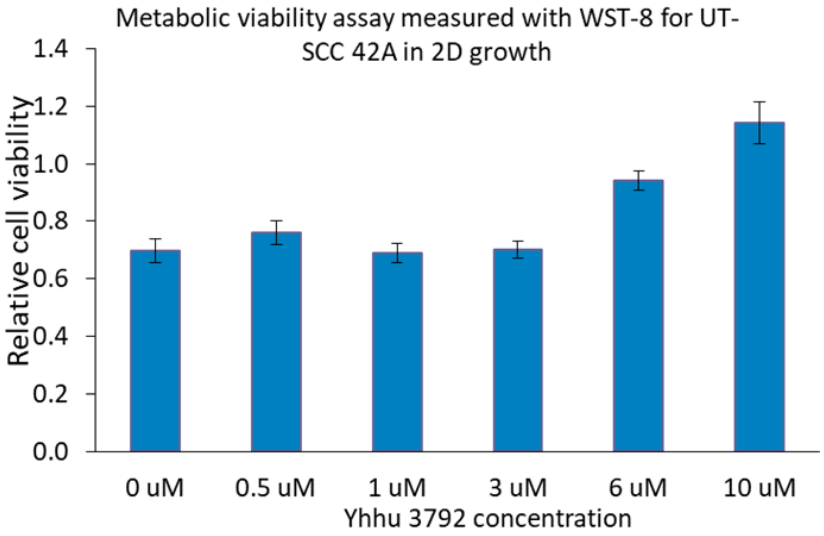

Figure 13. Effect of Yhhu 3792 on cell proliferation and viability for UT-SCC 42A in 2D monolayer culture. A) representative live cell images for Yhhu 3792 treated UT-SCC 42A in 2D culture. Cells were plated on day 0. Drug was added on day 1. The representative images shown were taken from the cells before the drug was added (day 1), and after 72h (day 4) of drug treatments. For the control treatments (0 µM), DMSO was added as vehicle control. The magnification is 10x. B) Proliferation curve (cell culture confluence) of UT-SCC-42A treated with Yhhu 3792. Number of replicated wells is 5. C) Cell metabolic viability for Yhhu 3792 treated UT-SCC-42A in 2D culture (measured on day 4). n = 5.

Nevertheless, in contrast to what we observed in 2D culture, for the cells grown in 3D cultures, Yhhu 3792 dramatically decreased the cell viability for the cells in Matrigel. The size of the organoids was significantly smaller at higher drug concentrations (10, 20 µM) (Figure 14, Appendix V). With longer treatment of 20 µM of Yhhu 3792 (Day 10, Figure 14A), the cell growth was restricted completely, and programmed cell death (apoptosis) or another form of cell death had likely occurred. For the cells embedded in Myogel, Yhhu 3792 prohibited the initial formation of organoids and seemingly facilitated the collective invasions at higher concentrations (10 and 20 µM) (Figure 15, Appendix VI).

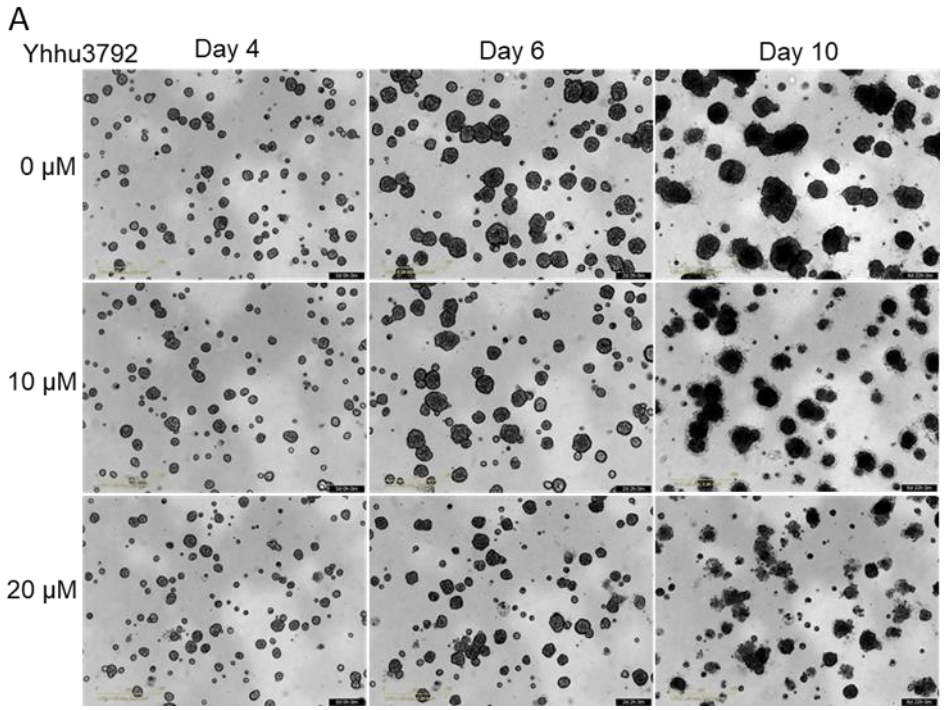

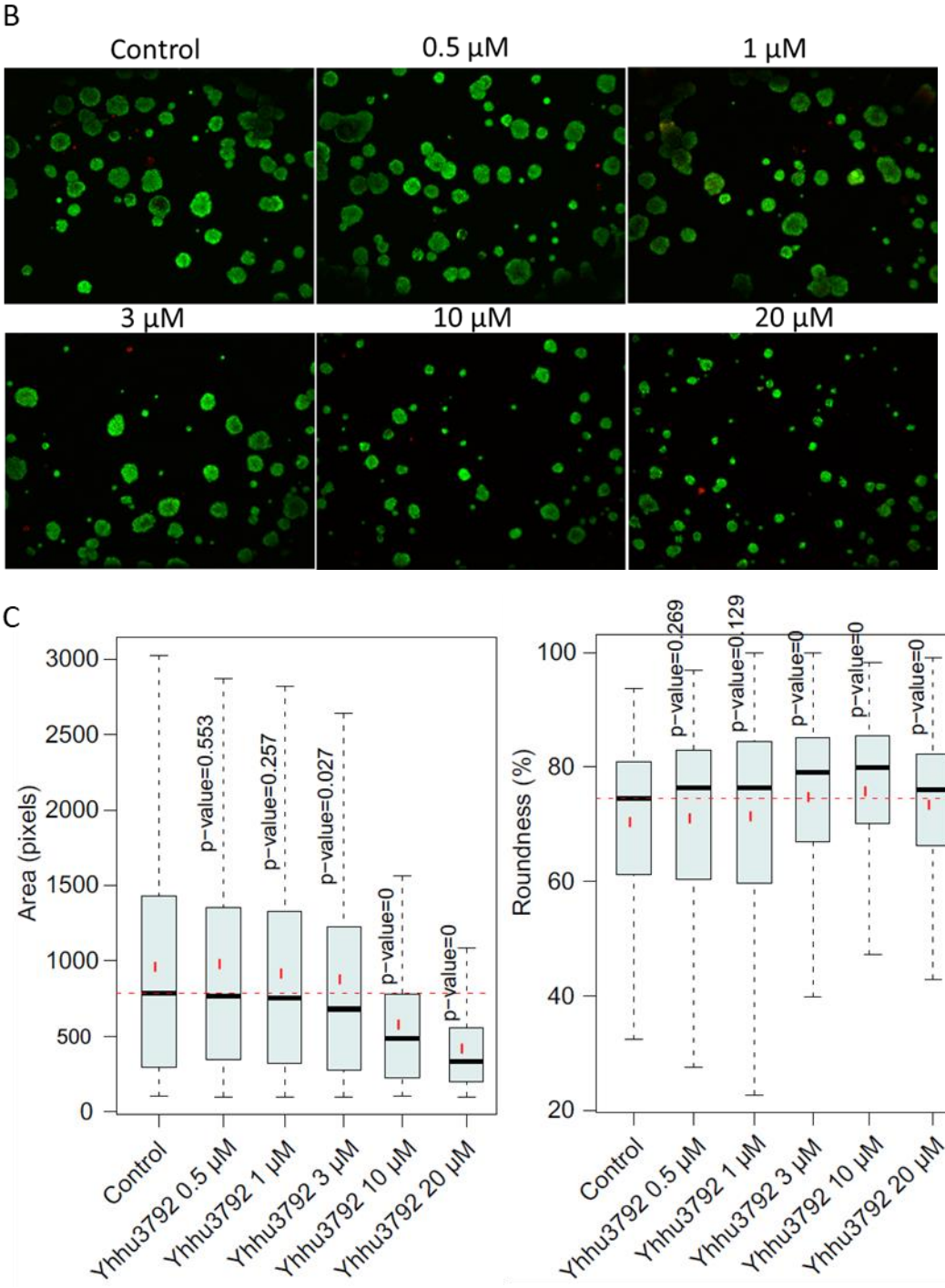
B
Control
0.5 µM
1 µM
3 µM
10 µM
20 µM
C
Area (pixels)
3000
2500
2000
1500
1000
500
0
p−value=0.553
p−value=0.257
p−value=0.027
p−value=0
p−value=0
Control
Yhhu3792 0.5 µM
Yhhu3792 1 µM
Yhhu3792 3 µM
Yhhu3792 10 µM
Yhhu3792 20 µM
Roundness (%)
100
80
60
40
20
p−value=0.269
p−value=0.129
p−value=0
p−value=0
p−value=0
Control
Yhhu3792 0.5 µM
Yhhu3792 1 µM
Yhhu3792 3 µM
Yhhu3792 10 µM
Yhhu3792 20 µM

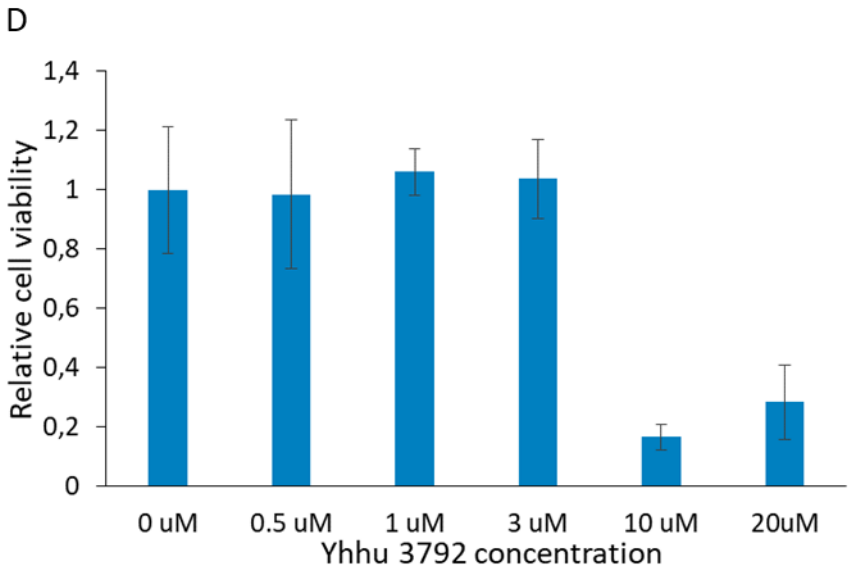

Figure 14. Effect of Yhhu 3792 on cell growth, viability and phenotypic changes for UT-SCC-42A cells in Matrigel. A) Representative live cell images of Yhhu treated cells in Matrigel, measured by IncuCyte. Cells were embedded on day 0. Drug was added on day 4 and the images shown were taken before the drug was added (Day 4), and after 48h (Day 6) and on day 10 (Day 10). For the cells where no drug was added, DMSO was added as vehicle control. The magnification is 10x. B) Confocal images of Calcein AM (green) and EthD-2 (red) stained organoids. Images were captured on day 10. The magnification is 5 x. C) Quantitative image analysis for Yhhu 3792 treated cells in Matrigel in 3D culture by AMIDA. Boxplots show the difference between the drug treated and control for the selected features (i.e., area, roundness). Black bar is median, red dot is mean. The statistics that AMIDA plots show are multiple-sample corrected t-test against control. $p < 0.05$ is considered as significant different. D) Cell metabolic viability of Yhhu 3792 treated cells in Matrigel in 3D culture (measured on day 11). $n = 5$.

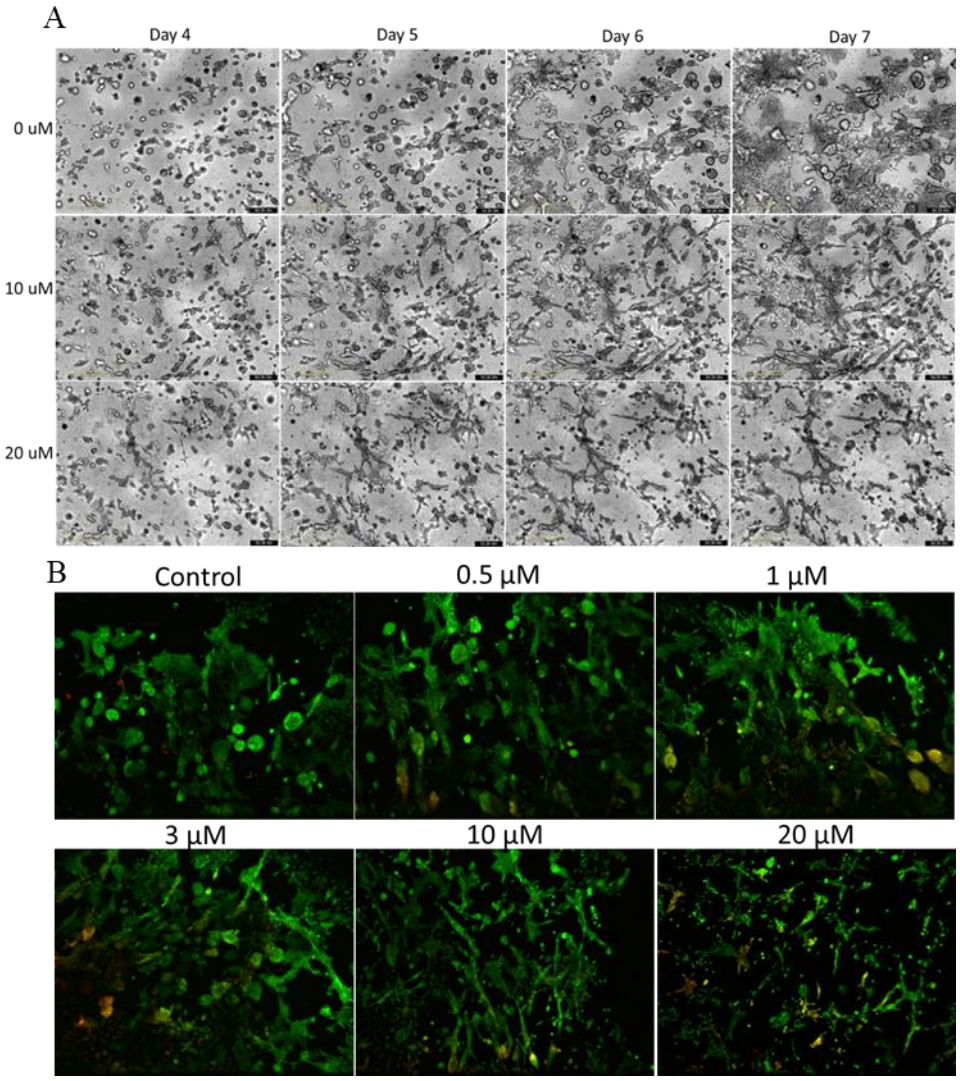

Figure 15. A) Representative live cell images of Yhhu 3792 treated UT-SCC-42A in Myogel, measured by IncuCyte. Drug was added on day 4 and the images shown were taken before drug was added (on day 4), after 24h (day 5), 48h (day 6), and 72h (day 7) of drug treatments. For the cells where no drug was added, DMSO was added as vehicle control. The magnification was 10 x. B) Confocal images of Calcein AM (green) and EthD-2 (red) stained organoids. Images were captured on day 7. The magnification is 5 x.

4.3 Verification of PSMD2 and DVL3 expressions in cell lines by qPCR and western blot

Before moving to study the correlation/regulation between Notch and PSMD2 or DVL3, we first did western blots to check whether PSMD2 and DVL3 are expressed in our

studied models. As seen from the western blots and qPCR results, PSMD2 and DVL3 are expressed in all our cell lines at both protein and mRNA level (Figure 16). The UT-SCC-42A and B cell lines had somewhat higher PSMD2 expression compared to UT-SCC-24A and B cell lines, and no significant difference in DVL3 expression was observed between these cell lines. This conclusion was identical based on both protein (Figure 16A) and mRNA expression levels (Figure 16B). The expression of PSMD2 and DVL3 in our studied models provided us a good basis for further study of the regulatory correlation of these two genes to Notch expression and its molecular functions, which will be discussed in the following sections.

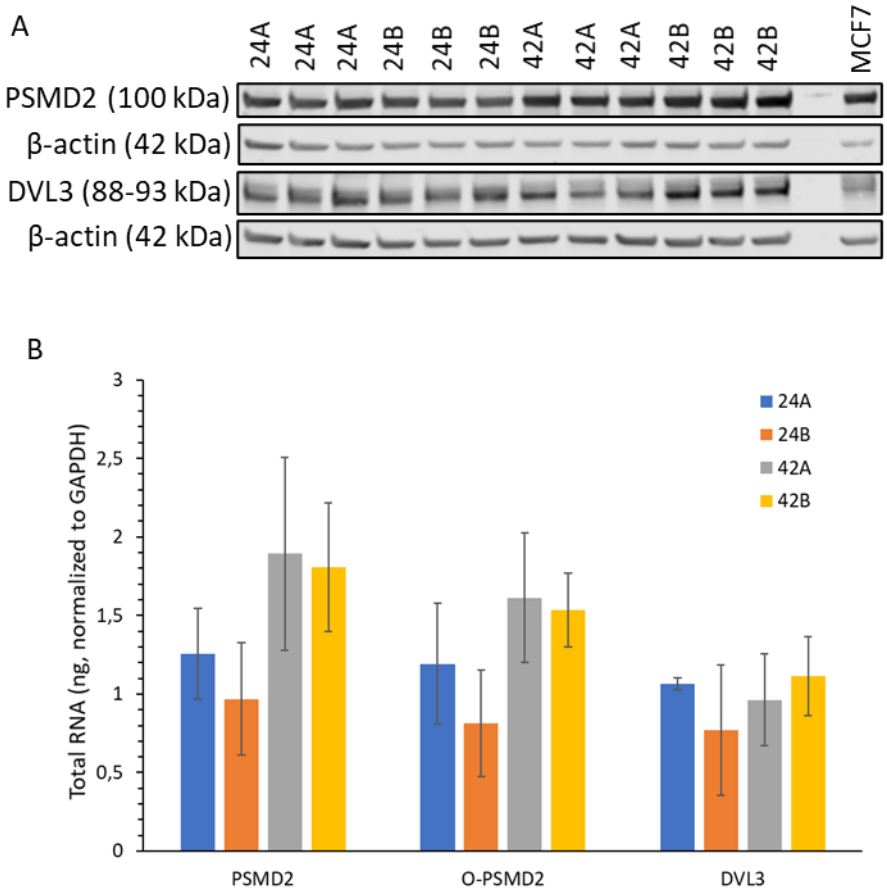

Figure 16. A) Western blots of PSMD2 and DVL3 in the studied UT-SCC cell lines. B) qPCR results for PSMD2 and DVL3 expressions in the cell lines. PSMD2 is self-designed primer, O-PSMD2 is commercial primer bought from OriGene. Two PSMD2 primers gave similar results. n = 3.

4.4 Possible regulation of PSMD2/DVL3 expression by Notch signaling

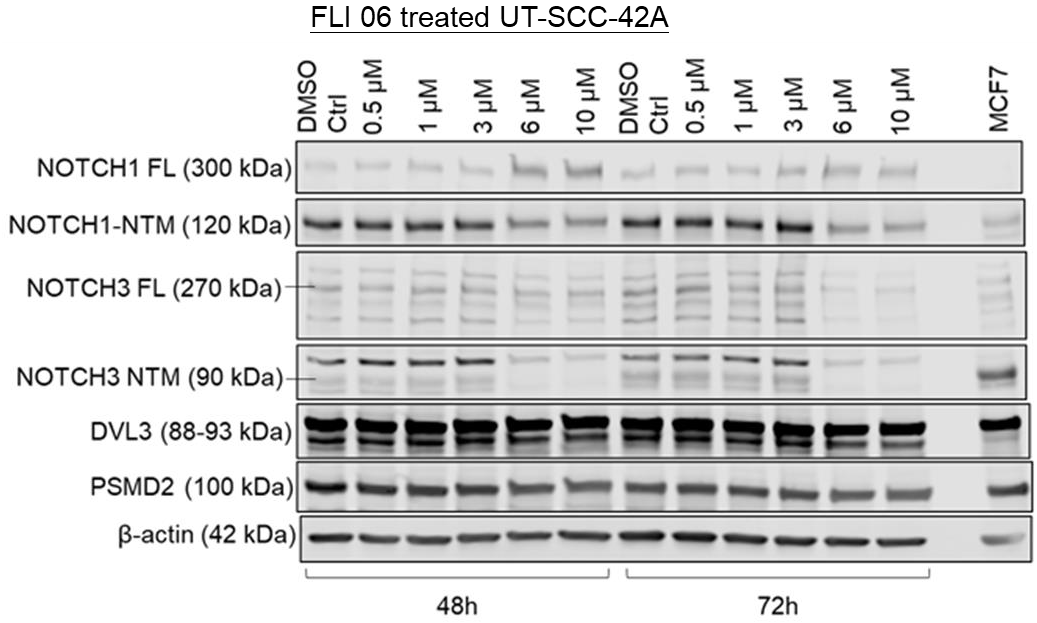

Figure 17. Western blots of NOTCH1, NOTCH3, DVL3, and PSMD2 for UT-SCC 42A cells treated with FLI-06 inhibitor after 48h and 72h. In this experiment, FLI 06 was used to evaluate the regulation of PSMD2 and DVL3 by Notch signaling. The drug concentrations used were 0, 0.5, 1, 3, 6, 10 µM.

The possible regulation of DVL3 by Notch was studied by western blotting. As seen from Figure 17, when NOTCH1 activation and Notch signaling activity (Figure 8A) was inhibited with 6 or 10 µM of drug treatment, there was no significant change on the expression level of PSMD2 and DVL3, which means that there is likely no regulation of PSMD2/DVL3 expression by Notch pathway.

4.5 Possible regulation of Notch signaling by PSMD2/DVL3

To investigate the possible regulation of Notch signaling by DVL3/PSMD2, we first performed an optimization of siRNA transfection to find out the most effective siRNA with optimal concentrations. As seen from Figure 18, the 4 DVL3 siRNA had similar efficiency with an estimate knock-down efficiency of 60-70% at 48h after transfection,

whereas siRNA transfection of PSMD2 was not so efficient in this experiment and needs to be further optimized and studied later.

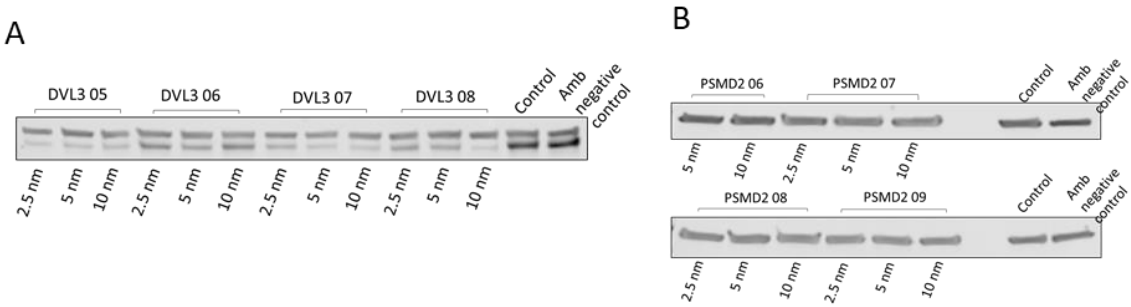

Figure 18. Optimization of siRNA transfections for UT-SCC-42A cells. Western blot analysis. A) Four different siRNA molecules to target DVL3 were used at three concentrations (2.5, 5, 10 nM). Ambion negative control siRNA #2 was used with 10 nM concentration. The samples were harvested 48h after transfection. B) Similar experimental setting for PSMD2 as described for A.

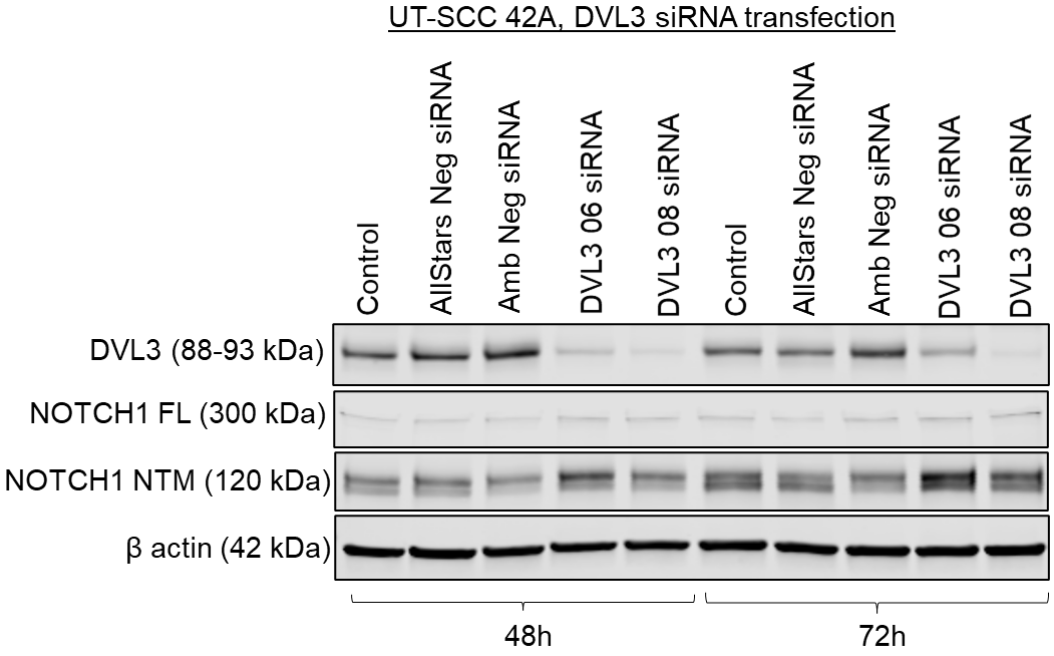

Figure 19. Western blot results for DVL3 06 and DVL3 08 siRNA transfected cells. The concentration used for DVL3 06 and DVL 08 siRNAs were 5 nM. Two scrambled siRNA controls were used with 5 nM concentration.

Next, to address the question whether Notch signaling is regulated by DVL3, we used DVL3 06 and DVL3 08 siRNAs to silence/knock down DVL3 in our cell line and looked

at the protein expression of NOTCH by wester blots. As seen from Figure 19, both siRNAs had knocked down DVL3 quite effectively with a knockdown efficiency of 70% and 90% at 48h, and 60% and 90% at 72h after the cell was transfected (Appendix VII). Knocking down of DVL3 significantly increased both cleaved (NTM) and inactive (full length) NOTCH1 expression level after 48 and 72h silencing (Appendix VII). This suggests that DVL3 is probably regulatory to NOTCH1 activity.

4.6 The effect of DVL3 knock down on cell growth pattern in 2D and 3D culture

With respect to the effect of DVL3 knock down on cell growth pattern in 2D and 3D culture, knocking DVL3 down did not seem to affect the morphology or cell growth in 2D culture (Appendix VIII), and no morphological sign of cytotoxicity was observed within 72h. In 3D Matrigel, negative siRNA controls and DVL3 06 siRNAs did not affect the cell morphology significantly except the symmetry of the organoids were slightly decreased (Figure 20B, roundness). It appears that DVL3 08 siRNA transfected cells tend to grow in significantly larger organoids than the mock-transfected controls (Figure 20A). In Myogel, the transfected cells grew in more stellate structures and form more easily monolayer growth at the bottom of the gel than untransfected cells (Figure 20A). The two negative controls used in this experiment had no clear effect on cell morphology. Nevertheless, the cell density of the "Ambion negative control" transfection was slightly lower, especially compared to the other negative control (AllStars siRNA control).

AMIDA analysis shows that two DVL3 siRNAs resulted in slightly opposite effects on the size (Area) and symmetry (Roundness) of the spheorids formed in Matrigel (Figure 20B). The opposite effects were also observed with metabolic assays (Figure 20C). In addition, it was noticed that the negative controls may cause some adverse effects to cell growth and viability. For example, Ambion negative siRNA decreased the symmetry (Roundness) of the organoids formed in Matrigel and the cell viability in both Matrigel and Myogel.

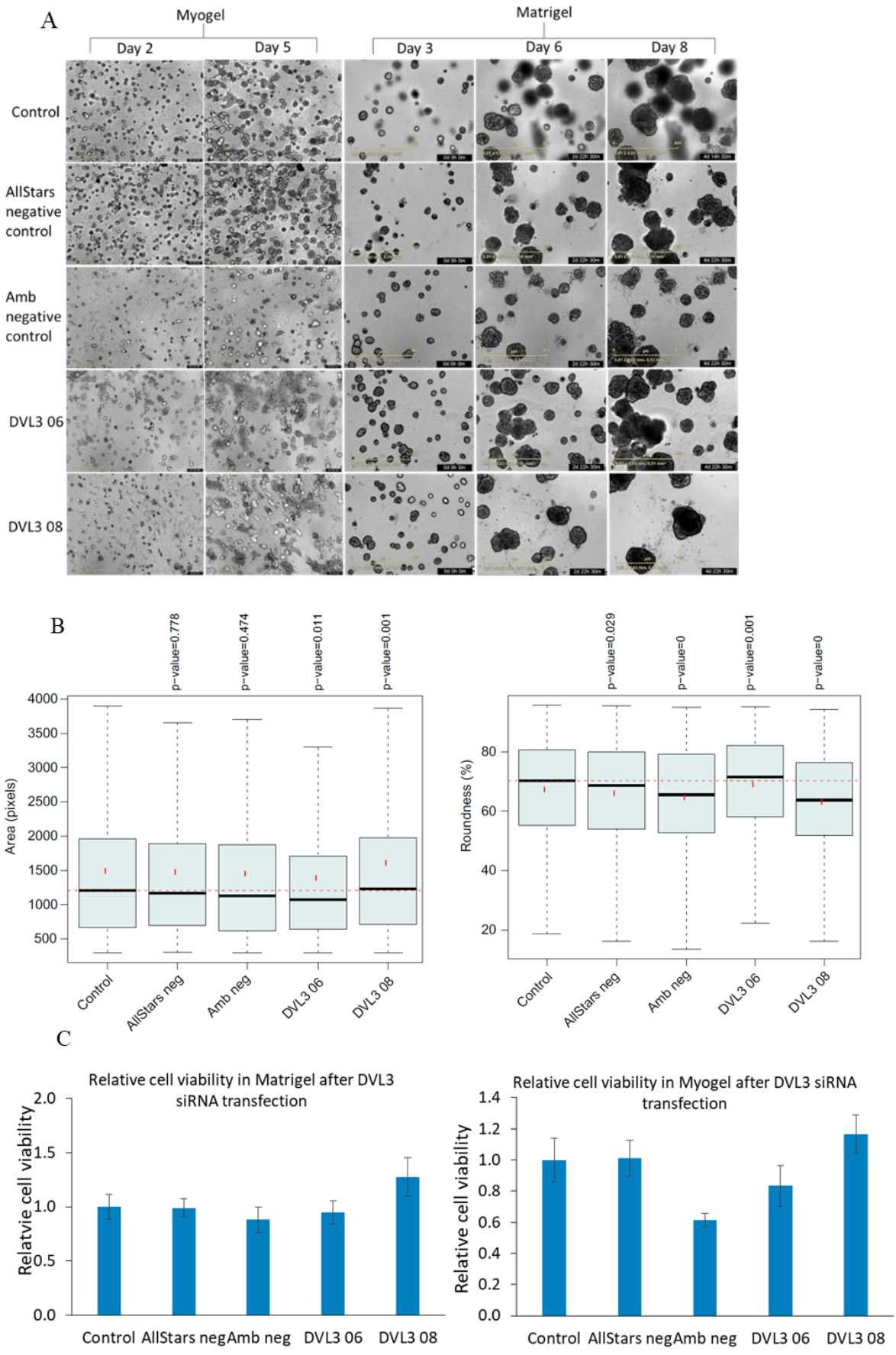

Figure 20. Effect of knocking down of DVL3 on cell functionality and morphological changes. A) Representative live cell images for controls (Control, AllStars negative

control, Amb negative control) and DVL3 siRNA (DVL3 06, DVL3 08) transfected cells in Matrigel and Myogel measured by IncuCyte. The cells from controls and those transfected were trypsinized 24h after transfection and embedded into Matrigel or Myogel in 3D culture on day 0. Images shown here were taken on day 2 (72h after transfection, 48h in 3D culture, marked as Day 2 in the images), and day 5 (Day 5) for the cells in Myogel. For the cells in Matrigel, the images shown were taken on day 3 (96h after transfection, 72h in 3D culture, marked as Day 3 in the images), day 6 (Day 6) and day 8 (Day 8). The image scale is different for Matrigel and Myogel. B) Quantitative image analysis for controls and DVL3 siRNA transfected cells in Matrigel in 3D culture by AMIDA. Boxplots show the difference between the transfected (or the negative control) and control for the selected features (i.e., area, roundness). Black bar is median, red dot is mean. The statistics that AMIDA plots show are multiple-sample corrected t-test against control. $p < 0.05$ is considered as significant different. C) Cell metabolic viability of controls and transfected cells in Matrigel (measured on day 9) and Myogel (measured on day 6). Data are shown as mean ± s.d. n = 12.

4.7 Expression of PSMD2 and DVL3 in HNSCC patient samples

The expression of PSMD2 and DVL3 in our HNSCC tumor and benign patient samples were examined by real-time qPCR. There was only a trend, but no significant difference in DVL3 expression observed between the studied tumor and benign tissues (Wilcoxon signed-rank test, p value = 0.24). Altogether, 11 out of 17 matched tumor/benign tissue pairs, in which DVL3 showed higher/slightly higher expression in the tumor compared to benign tissue. However, interestingly, we observed a very significant differential expression of PSMD2 between tumor and normal tissues (p value = 0.014), indicating that PSMD2 is most likely overexpressed more in a major portion of the tumors.

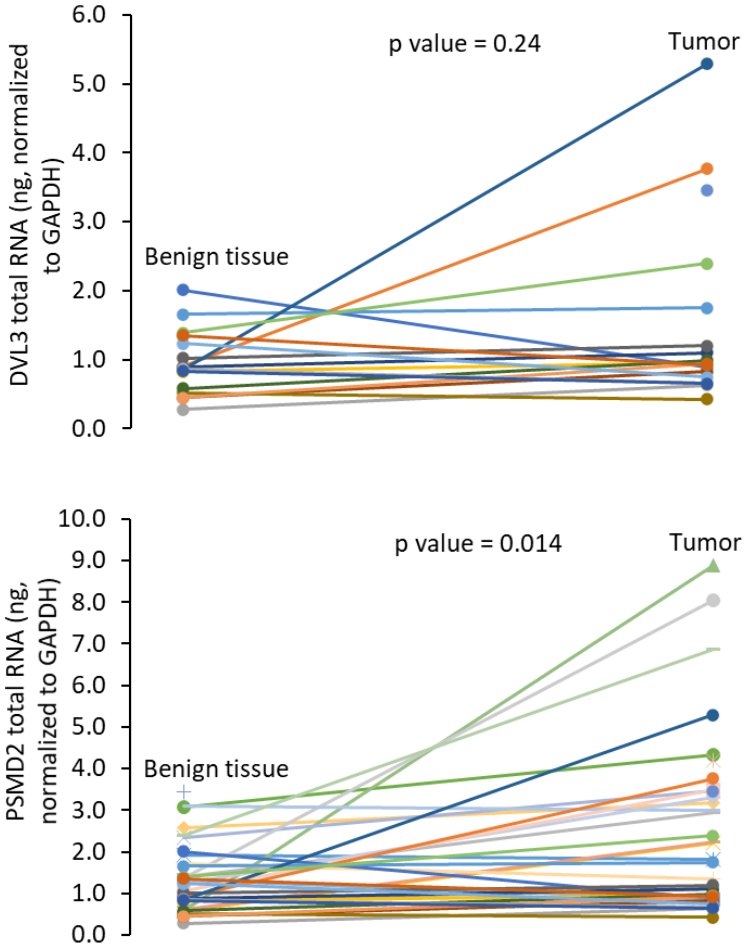

Figure 21. DVL3 and PSMD2 total RNA amount in HNSCC benign tissue vs. tumor.

5. DISCUSSION

5.1 Notch activity and expression of DVL3 and PSMD2 in UT-SCC cell lines

In this work, the Notch activation and expression of DVL3 and PSMD2 in the UT-SCC cell lines was evaluated by using western blotting and qPCR. They were found all expressed in our studied models with higher NOTCH expression in UT-SCC-24 cell lines (from tongue). PSMD2 however, was expressed more strongly in UT-SCC-42 cell lines (from larynx). The variations in these gene expressions show that these are tumor and cell line specific. UT-SCC-24A and B are derived from primary and metastatic tongue squamous cell carcinoma, UT-SCC-42A and B are derived from primary and metastatic laryngeal carcinoma, of the same patient, respectively. It is expected that primary and secondary/metastatic tumors (and the cell lines derived from these) show differential gene

signatures that may correlate with differential aggressiveness. Since no NOTCH1 mutation in UT-SCC-42A (Lepikhova et al., 2018) was detected, and interesting phenotypes was found in the previous studies (unpublished data), this line was selected as the base model to study the functional role of NOTCH and potential NOTCH associated genes (PSMD2, DVL3) in HNSCC. The drawback of this cell line is the low expression level of NOTCH3. Regarding to this, a better candidate could be 24A in which both NOTCH1 and NOTCH3 are highly expressed.

5.2 Differential Notch inhibition and activation by drug treatments

In this work, in order to study the functional role of Notch in HNSCC, we used the compounds FLI 06 and Yhhu 3792 to inhibit or activate Notch signaling, respectively. The major and most widely used NOTCH inhibitors are γ-secretase inhibitors (GSI) and monoclonal antibodies, targeting either NOTCH receptors or ligands. The compound dihydropyridine FLI 06 used in this work is not a GSI but acts as a specific inhibitor that disrupts Notch trafficking from the Golgi apparatus to the cell membrane and prevents the early secretion (a step before exit from the endoplasmic reticulum) of functional full length NOTCH protein, and thereby blocks functional Notch signaling (Lu et al. 2018; Krämer et al. 2013). The compound FLI 06 has been shown to suppress the protein expression of NOTCH receptor, and the mRNA expression of NOTCH1, NOTCH2 (Gan et al, 2019). In addition, HEY1, HES1 and HEY2 protein and mRNA expression were found downregulated when tongue cancer cells were treated for 48h with FLI 06 (Gan et al, 2019). In our study, FLI 06 restrained the activation of NOTCH1 and NOTCH3 expression, and downregulated, HES1 and HES5 in primary laryngeal carcinoma cells (UT-SCC-42A) at concentrations exceeding > 3 μM after a drug exposure of 48h. This is in line with the previous findings by Gan et al. (Gan et al., 2019), which have proved that FLI 06 is a valid and functional Notch inhibitor perfectly suited for our studies and model systems. With respect to Yhhu 3792, NOTCH1 signaling was not activated as expected and previously reported, at least not after 48h of drug treatment. Instead, a slight but reproducible decrease in NOTCH3 activation, HES1 and HES5 expression, was observed. To our knowledge, there has not been any study related to the effects of Yhhu 3792 on Notch signaling in HNSCC. Although Yhhu 3792 has been reported to activate the Notch signaling in neuronal stems cells (Lu et al., 2018), but the mechanism is unclear. In our

study, it is speculated that the drug may have affected other "off target" signaling pathways. For instance, EGFR activation can promote its downstream, such as MAPK/ERK, PI3K signaling pathways, which are frequently mutated in HNSCC. In this work, it was found that the p-ERK1/2 expression of UT-SCC-42A was increased/decreased after 24h/48h Yhhu 3792 treatment (Figure 22). However, since the main interest of our study was to use of specific modulators of Notch signaling including drugs and siRNAs to evaluate the assumed functional role of DVL3 and PSMD2 on the NOTCH pathway, the mechanism by which Yhhu 3792 may work is beyond the focus of the current study.

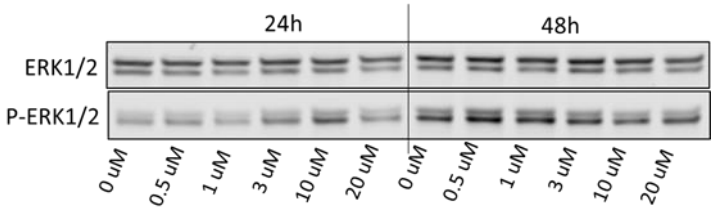

Figure 22. p-ERK1/2/ERK1/2 expression in Yhhu 3792 treated UT-SCC-42A.

5.3 Inhibition of Notch signaling affects cell growth pattern and reduces cell proliferation and viability

Inhibition of Notch signaling by FLI 06 significantly decreased cell proliferation and reduced cell viability in both 2D and 3D culture (in Matrigel and Myogel). In 2D cultures, the cells formed round or polygonal shapes with typical flat structures. In Matrigel, the same cells formed multicellular and typically well organized, partially differentiated organoids, while in Myogel, the cells were much more invasive and formed simultaneously round multicellular aggregates, and irregular, spindle-like structures of varying sizes and dimensions. The different phenotypes observed in Myogel vs Matrigal are likely due to the 3D culture conditions and the effect of the extracellular matrices, specifically the presence of ECM proteins like collagens and laminins. A study by Wahbi et al. show that HNSCC cell morphology and the gene expression/signature can be very strongly affected by the type of matrix used (Wahbi et al., 2022).

In this work, we found that when Notch activity is decreased, the spheroids in Matrigel become smaller and less symmetric and the overall viability is decreased. In Myogel, the

spindle/branch structures are diminished when there is a reduction in Notch activity, and the organoids formed become smaller, more irregular, or apoptotic. Which means, inhibition of Notch signaling by FLI 06 inhibits the cell invasion in Myogel. On the other hand, Yhhu 3792, as a NOTCH activator, (which did not work in our case, or probably had an opposite effect) results in quite different effects on cell growth in 2D versus 3D culture. In 2D culture, Yhhu 3792 slightly decreases the proliferation rate but increases the cell metabolic viability. Yhhu 3792 also decreases the cell growth and viability in Matrigel, the organoids become smaller along with likely programmed cell death (apoptosis) or another form of cell death. Interestingly, the cells in Myogel after Yhhu 3792 treatments form less organoids but more spindle/stretched structures which means, the cells become more invasive after Yhhu 3792 treatment. This spindle-like morphology may manifest an epithelial-mesenchymal transition, which can contribute to cancer cell migration and invasion (Wahbi et al., 2022; Son and Moon, 2010; Kalluri and Weinberg, 2009; Zhou et al., 2017).

5.4 Potential regulation between DVL3/PSMD2 and Notch signaling

Regarding to the potential regulation between DVL3 or PSMD and Notch signaling, it was found that NOTCH does NOT regulate expression of either DVL3 or PSMD2. On the contrary, DVL3 may be regulatory to Notch activity. According to literature, Notch signaling can crosstalk with Wnt signaling pathway via Dishevelled proteins. Dishevelled proteins can inhibit both canonical and non-canonical Notch signaling (Axelrod et al., 1996). Alfred and Vaccari found that the levels of NOTCH expression and activity are frequently inversely correlated with those of β catenin (Alfred and Vaccari, 2018). It was also reported that there might be transcriptionally regulation of Notch-pathway-related genes by the Wnt cascade (Ungerbäck et al., 2011; Kaemmerer et al., 2019). In addition, a study by Lee et al. showed that NOTCH1 acted the upstream of canonical Wnt signaling in HNSCC cells, suppression of NOTCH1 reduced nuclear β-catenin levels in Wnt signaling in HNSCC (Lee et al., 2016). Furthermore, it was reported that the multi-domain Dishevelled proteins can bind and reduce the CSL level of active transcription factors and thus inhibit formation of NICD activator complex (Collu et al., 2012; Alfred and Vaccari, 2018; Kaemmerer et al., 2019). In our study, it was found that knocking down of DVL3 increases NOTCH1 expression and activation. However, the mechanism behind is not

known. It might have something related to Wnt pathway and/or β-catenin, which could be one of the interesting studies in the future.

5.5 Knocking down of DVL3 affects cell growth and viability

In this chapter, we will discuss about the functional role of DVL3 in cell growth and viability in our study cell line (UT-SCC-42A, larynx squamous cell carcinoma). DVL3, as one of the Dishevelled proteins, is involved in both Notch and Wnt signaling. In this work, we have found that it may be regulatory to Notch activity. To our knowledge, there is very limited study of the molecular role of DVL3 on cell growth and viability in HNSCC. In this work, we found that knocking down of DVL3 may affect cell growth and viability. Our preliminary results indicate that when DVL3 is knocked down the cells tend to grow in larger organoids in Matrigel and the cell viability is slightly improved in both Matrigel and Myogel in 3D culture. However, the two siRNAs used in this work gave slightly opposite results, one of which may have an off-target effect. Therefore, further experiments need to be conducted to clarify this issue.

5.6 Differential expression of PSMD2 and DVL3 in patient samples

In this thesis work, to explore the prognostic value of PSMD2 and DVL3 in HNSCC, we compared PSMD2 and DVL3 mRNA expression level in HNSCC tumor and adjacent benign tissues. Our results show that PSMD2 mRNA is expressed more in tumor tissues, but there is no significant difference in DVL3 mRNA expression between tumor and benign tissues in our patient cohort. However, differential expression of DVL3 in HNSCC tumor and adjacent non-cancer tissues have been reported by Zhao et al. (Zhao et al., 2020). In the patient cohort we studied, the expression of DVL3 in 11 out of 17 matched tumor/benign pairs are slightly higher/higher in the tumor than in benign tissue. In addition, the comparison may be affected by the number of samples analyzed and the tissue compositions from different locations (see the list of the patient samples in Table 1). Therefore, our next step is to look further into the expression level of PSMD2 and DVL3 in a larger patient cohort.

6. CONCLUSIONS

In summary, NOTCH has been found to be active and functional in all the studied UT-SCC cell lines. The inhibitor, FLI 06, used in this study at least partially reduced Notch activation and activity in UT-SCC-42 cell line. It seems Notch signaling plays as a tumor promoting role in this cell line. Inhibition of Notch signaling decreases cell proliferation, metabolic viability and induces cell apoptosis of UT-SCC-42A cells in both 2D and organotypic 3D cultures. The two selected target genes, DVL3 and PSMD2, are also highly expressed in our models, and it was found that PSMD2/DVL3 is not likely to be transcriptionally regulated by Notch signaling. However, DVL3 is most probably regulatory to Notch expression and activity. Our preliminary results show that knocking down of DVL3 significantly increases NOTCH1 expression and activation at the protein level, and it seems that altered cells tend to grow in larger organoids in 3D culture in Matrigel. In this study, we also found that PSMD2 is significant over-expressed in tumors. Next, we are interested to find out whether there is a regulatory association of Notch signaling to PSMD2 and what is the effect of knocking down of PSMD2 on tumor growth and cell viability in UT-SCC-42A. In addition, the expression level of PSMD2/DVL3 in our patient cohort will be associated with patient treatment response or prognosis to see whether they can be used as potential prognostic biomarkers. The scientific questions that have been addressed in this work and the future steps are summarized in below:

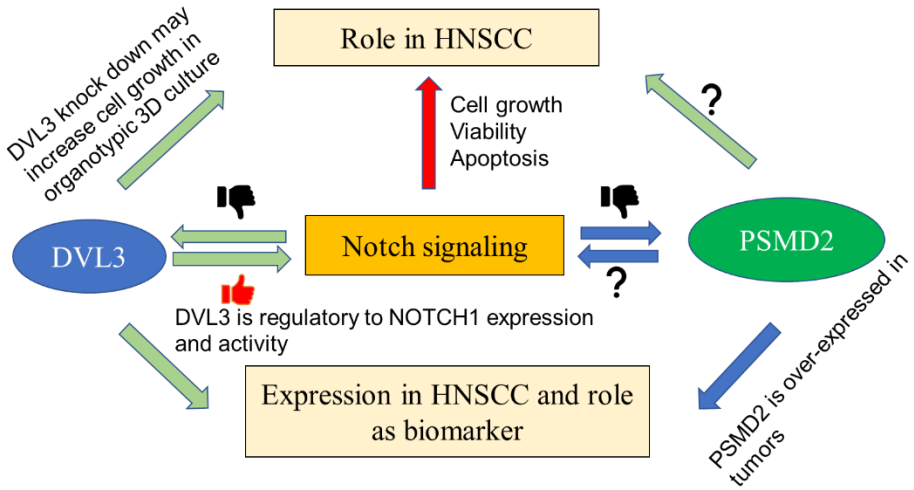

7. ACKNOWLEDGEMENTS

This thesis work was carried out at High Content Screening lab during 01.09.2021-15.3.2022 at Institute of Biomedicine, Faculty of Medicine, University of Turku.

I would like to thank Adjunct Professor Matthias Nees for giving me the opportunity to work in his lab and for his support and encouragement throughout this work. I would also like to express my great gratitude to Dr. Mervi Toriseva for her elaborate supervision and patience in guiding me throughout the whole experimental and thesis work. Without your help, this thesis would not have been possible. Thank also all "NOTCH" project members, Arkadiusz Czerwonka, Doriane Le Manach, Alinda Anameric, from University of Lublin for nice collaboration. Adjunct Professor Sami Ventelä from Turku Bioscience Centre, and M.D. Johannes Routila, both from Department of Otorhinolaryngology-head and neck surgery, University of Turku and Turku University Hospital, are acknowledged for providing us the patient samples and helping with the ethical issues. Notch Ko breast cancer cells used in gene expression data mining were kindly provided by the Cell Fate group (Sahlgren).

I am also truly thankful to research technician Minna Santanen for helping with the technical issues at Medisiina D. Docent Liisa Nissinen is thanked for sharing her knowledge on western blotting.

My great gratitude also to Nees group members, Docent Malin Åkerfelt, Jesse Mattsson, Syeda Afshan, Erica Långbacka, Vladyslav Melnyk, for sharing your thoughts during lab meetings and helping with all the practical issues in the lab. Thank you, Jesse Mattsson for expert technical support with confocal microscopy and AMIDA analysis.

I would also like to thank all BIMA board members, Diana Toivola, Riku Klén, Elnaz Fazeli, for accepting me into this programme so that I had the chance to enter the imaging world and start a new scientific journey. Thank all the coordinators, Raili Kronström, Joanna Pylvänäinen, Dado Tokic, for helping with all the study related issues.

My warm thanks to my friends in Turku: Wang Fan, Qiao Xi, Na Li, Haolin Lu, Wenyang Xu, Xue Zhang, Pingping Su, Chunlin Xu, Xiaoju Wang, for your friendship and supports.

Last, I want to thank my parents and my parents-in-law for their endless love and logistic support. My dearest family, my husband, Bingzhi Li, my lovely sons, Yicheng and

Shucheng, thank you for your love and smiles, which have been always a power for me to move on.

8. REFERENCES

Ahonen, I., M. Åkerfelt, M. Toriseva, E. Oswald, J. Schüler, and M. Nees. 2017. A high-content image analysis approach for quantitative measurements of chemosensitivity in patient-derived tumour microtissues. *Scientific reports.* 7: 6600.

Alfred, V., and T. Vaccari. 2018. Mechanisms of non-canonical signalling in health and disease: diversity to make therapy up to a Notch? In *Molecular Mechanisms of Notch Signalling* (edited by Borggrefe T and Giaimo D), pp.187-204. Springer, Cham, Switzerland.

Artavanis-Tsakonas, S., M.D. Rand, and R.J. Lake. 1999. Notch signalling: cell fate control and signal integration in development. *Science*. 284(5415): 770-776.

Aster, J.C., W.S. Pear, and S.C. Blacklow. 2017. The varied roles of Notch in cancer. *Annu Rev Pathol.* 12: 245-275.

Auperin, A. 2020. Epidemiology of head and neck cancers. *Curr. Opin. Oncol.* 32: 178-186.

Axelrod J.D., K. Matsuno, S. Artavanis-Tsakonas, and N. Perrimon. 1996. Interaction between Wingless and Notch signaling pathways mediated by dishevelled. *Science.* 271(5257): 1826-1832.

Buddavarapu, T. Sanford, A. Choudhary, W. Darden, A. Adai, G. Latham, J. Bishop, R. Sharma, W.H. Westra, P. Hennessey, C.H. Chung, and J.A: Califano. 2013. *Cancer Research.* 74(4): 1091-1104.

Celebi, A., C. Orhan, B. Seyhan, and N. Buyru. 2020. Silencing of Wwox increases nuclear import of Dvl proteins in head and neck cancer. *Journal of Cancer*. 11: 4030-4036.

Chow, L.Q.M. 2020. Head and neck cancer. *N. Engl. J. Med.* 382: 60-72.

Collu, G.M., A. Hidalgo-Sastre, A. Acar, L. Bayston, C. Gildea, M.K. Leverentz, C.G. Mills, T.W. Owens, O. Meurette, K. Dorey, and K. Brennan. 2012. Dishevelled limits Notch signalling through inhibition of CSL. *Development*. 139(23): 4405-4415.

Cox, T.R. 2021. The matrix in cancer. *Nat Rev Cancer*. 21: 217-238.

Frankland-Searby, S. and S.R. Bhaumik. 2012. The 26S proteasome complex: an attractive target for cancer therapy. *Biochim Biophys Acta. January.* 1825(1): 64-76.

Fukusumi, T., T T.W. Guo, and A. Sakai. 2018. The NOTCH4 – HEY1 Pathway induces epithelial mesenchymal transition in head and neck squamous cell carcinoma. *Clin Cancer Res.* 24(3):619–633.

Gan, R.H., H. Wei, J. Xie, D.P. Zheng, E.L. Luo, X.Y. Huang, J. Xie, Y. Zhao, L.C. Ding, B.H. Su, L.S. Lin, D.L. Zheng, and Y.G. Lu. 2018. Notch1 regulates tongue cancer cells proliferation, apoptosis and invasion. *Cell Cycle*. 17(2): 216-224.

Gan, R.H., L.S. Lin, J. Xie, L. Huang, L.C. Ding, B.H. Su, X.E. Peng, D.L. Zheng, and Y.G. Lu. 2019. FLI-06 intercepts Notch signalling and suppresses the proliferation and self-renewal of tongue cancer cells. *OncoTargets and Therapy*. 12: 7663-7674.

Greenwald, I. 2012. Notch and the awesome power of genetics. *Genetics.* 191(3): 655-669.

Grenman, R., K. Pekkola-Heino, H. Joensuu, K. Aitasalo, P. Klemi, and T. Lakkala. 1992. UT-MUC-1, a new mucoepidermoid carcinoma cell line, and its radiosensitivity. *Arch Otolaryngol Head Neck Surg*. 118: 542–7.

Hagemann, J.C. Jacobi, M. Hahn, V. Schmid, C. Welz, S. Schwenk-Zieger, R. Stauber, P. Baumeister, and S. Becker. 2017. Spheroid-based 3D cell cultures enable personalized therapy testing and drug discovery in head and neck cancer. *Anticancer Res.* 37(5): 2201-2210.

Hughes, C.S., L.M. Postovit, and G.A. Lajoie. 2010. Matrigel: a complex protein mixture required for optimal growth of cell culture. *Proteomics.* 10: 1886-1890.

Härmä, V., J. Virtanen, R. Mäkelä, A. Happonen, J.P. Mpindi, M. Knuuttila, P. Kohonen, J. Lötjönen, O., Kallioniemi, and M. Nees. 2010. A comprehensive panel of three-dimensional models for studies of prostate cancer growth, invasion and drug responses. *PLoS ONE*. 5(5): e10431.

Härmä, V., H.P. Schukov, A. Happonen, I. Ahonen, J. Virtanen, H. Siitari, M. Åkerfelt, J. Lötjönen, and M. Nees. 2014. Quantification of dynamic morphological drug responses in 3D organotypic cell cultures by automated image analysis. *PLoS ONE*. 9(5): e96426.

Johnson, D.E., B. Burtness, C. Rene Leemans, V.W. Yan Lui, J.E. Bauman and J.R. grandis. 2020. Head and neck squamous cell carcinoma. *Nature reviews. Disease primers*. 6: 92.

Jung, S.Y., S. Seolwha, E. Kang, D.Y. Noh, and W. Han. 2016. Abstract B22: PSMD2 is a molecular marker for a poor prognosis and determines cancer stem cells traits in breast cancer. *Molecular cancer research*. 14: B22-B22.

Kaemmerer, E., M. Kyung Jeon, A. Berndt, C. Liedtke, and N. Gassler. 2019. Targeting Wnt signalling via Notch in intestinal carcinogenesis. *Cancers.* 11: 555.

Kalafut J., A. Czerwonka, A. Anameric, A. Przybyszewska-Podstawka, J.O. Misiorek, A. Rivero-Müller, and M. Nees. 2021. Shooting at Moving and Hidden Targets-Tumour Cell Plasticity and the Notch Signalling Pathway in Head and Neck Squamous Cell Carcinomas. *Cancers.* 13(24): 6219

Kalluri, R., and R.A. Weinberg. 2009. The basics of epithelial-mesenchymal transition. *Journal of Clinical Investigation.* 119(6): 1420-1428.

Katoh, M., and M. Katoh. 2020. Precision medicine for human cancers with Notch signalling dysregulation (Review). *International Journal of Molecular Medicine*. 45: 279-297.

Kayamori, K., K. Katsube, K. Sakamoto, Y. Ohyama, H. Hirai, A. Yukimori, Y. Ohata, T. Akashi, M. Saitoh, K. Harada, H. Harada, and A. Yamaguchi. 2016. NOTCH3 is induced in cancer-associated fibroblasts and promotes angiogenesis in oral squamous cell carcinoma. *PLoS One.* 11(4): e0154112.

Krämer, A., T. Mentrup, B. Kleizen, E. Rivera-Milla, D. Reichenbach, C. Enzensperger, R. Nohl, E. Täuscher, H. Görls, A. Ploubidou, C. Englert, O. Werz, H.D. Arndt, and C. Kaether. 2013.Small molecules intercept Notch signalling and the early pathway. *Nature chemical biology*. 9: 731-738.

Kumar, R., L. juillerat-Jeanneret, and D. Golshayan. 2016. Notch antagonists: potential modulators of Cancer and inflammatory diseases. *J Med Chem*. 59 (17): 7719-7737.

LaFoya, B., J.A. Munroe, M.M. Mia, M.A. Detweiler, J.J. Crow, T. Wood, S. Roth, B. Sharma, and A.R. Albig. 2016. Notch: a multi-functional integrating system of microenvironmental signals. *Dev. Biol.* 418: 227-241.

Lee, S.H., S.I. Do, H.J. Lee, H.J. Kang, B.S. Koo, and Y.C. Lim. 2016. Notch1 signalling contributes to stemness in head and neck squamous cell carcinoma. *Laboratory Investigation*. 96: 508-516.

Lepikhova, T., P.R. Karhemo, R. Louhimo, B. Yadav, A. Murumägi, E. Kulesskiy, M. Kivento, H. Sihto, R. Grenman, S.M. Syrjänen, O. Kallioniemi, T. Aittokallio, K. Wennerberg, H. Joensuu, and O. Monni. 2018. Drug-sensitivity screening and genomic characterization of 45 HPV-negative head and neck carcinoma cell lines for novel biomarkers of drug efficacy. *Mol Cancer Ther.* 17 (9): 2060-2071.

Li, Y., J. Huang, B. Zeng, D. Yang, J. Sun, X. Yin, M. Lu, Z. Qiu, W. Peng, T. Xiang, H. Li, and G. Ren. 2018. PSMD2 regulates breast cancer cell proliferation and cell cycle progression by modulating p21 and p27 proteasomal degradation. *Cancer Lett.* 430: 109-122.

Lin, J.T., M.K. Chen, K.T. Yeh, C.S. Chang, T.H. Chang, C.Y. Lin, Y.C. Wu, B.W. Su, K.D. Lee and P.J. Chang. 2010. Association of high levels of Jagged-1 and Notch-1 expression with poor prognosis in head and neck cancer. *Ann Surg Oncol.* 17: 2976-2983.

Iivneh, I., V. Cohen-Kaplan, C. Cohen-Rosenzweig, N. Avni, and A. Ciechanover. 2016. The life cycle of the 26S proteasome: from birth, through regulation and function, and onto its death. *Cell Res.* 26: 869-885.

Lu, H., G. Cheng, F. Hong, L. Zhang, Y.H. Hu, and L.Y. Feng. 2018. A novel 2-phenylamino-quinaoline-based compound expands the neural stem cell pool and promotes the hippocampal neurogenesis and the cognitive ability of adult mice. *Stem Cells.* 36: 1273-1285.

Lu, Z. Y. Ren, M. Zhang, T. Fan, Y. Wang, Q. Zhao, H.M. Liu, W. Zhao, and G. Hou. 2018. FLI-06 suppresses proliferation, induces apoptosis and cell cycle arrest by targeting LSD1 and Notch pathway in esophageal squamous cell carcinoma cells. *Biomedicine & Pharmacotherapy*. 107: 1370-1376.

Lubin, D.J., R. Mick, S.G. Shroff, K. Stashek, and E.E. Furth. 2018. The Notch pathway is activated in neoplastic progression in esophageal squamous cell carcinoma. *Hum Pathol.* 72: 66–70.

Marquez-Exposito, L., E. Cantero-Navarro, C. Lavoz, M. Fierro-Fernández, J. Poveda, S. Rayego-Mateos, R.R. Rodrigues-Diez, J. L. Morgado-Pascual, M. Orejudo, S. Mezzano, M. Ruiz-Ortega. 2018. Could Notch signalling pathway be a potential therapeutic option in renal diseases? *Nefrologia (Engl Ed).* 38(5): 466-475.

Matsuyama, Y., M. Suzuki, C. Arima, Q.M. Huang, S. Tomida, T. Takeuchi, R. Sugiyama, Y. Itoh, Y. Yatabe, H. Goto, and T. Takahashi. 2011. Proteasomal non-catalytic subunit

PSMD2 as a potential therapeutic target in association with various clinicopathologic features in lung adenocarcinomas. *Mol Carcinog.* 50: 301-309.

Megason, S.G., and S.E. Fraser. 2007. Imaging in systems biology. *Cell.* 130: 784-795.

Megason, S.G., and S.E. Fraser. 2003. Digitizing life at the level of the cell: high-performance laser-scanning microscopy and image analysis for in toto imaging of development. *Mechanisms of Development.* 120(11): 1407-1420.

Misiorek, J.O., A. Przybyszewska-Podstawka, J. Kalafut, B. Paziewska, K. Rolle, A. Rivero-Muller, and M. Nees. 2021.Context matters: Notch signatures and pathway in cancer progression and metastasis. *Cells*. 10: 94.

Mutvei, A.P., S.K.J. Landor, R. Fox, E.B. Braune, Y.L. Tsoi, Y.P. Phoon, C. Sahlgren, J. Hartman, J. Bergh, S. Jin, and U. Lendahl. 2018. Notch signalling promotes a HIF2α-driven hypoxic response in multiple tumour cell types. *Oncogene.* 37: 6083–6095.

Natsuizaka, M., K.A. Whelan, and S. Kagawa. 2017. Interplay between Notch1 and Notch3 promotes EMT and tumour initiation in squamous cell carcinoma. *Nat Commun*. 8(1): 1758.

Nyman, P.E., D. Buehler, and P.F. Lambert. 2018. Loss of function of canonical Notch signalling drives head and neck carcinogenesis. *Clin Cancer Res.* 24(24): 6308-6318.

Oswald, F., B. Täuber, T. Dobner, S. Bourteele, U. Kostezka, G. Adler, S. Liptay, and R.M. Schmid. 2001. P300 acts as a transcriptional coactivator for mammalian Notch-1. *Molecular and Cellular Biology*. 21 (22): 7761-7774.

Pai, V.C., C.C. Hsu, T.S. Chan, W.Y. Liao, C.P. Chuu, W.Y. Chen, C.R. Li, C.Y. Lin, S.P. Huang, L.T. Chen, K.K. Tsai. 2019. ASPM promotes prostate cancer stemness and progression by augmenting Wnt-Dvl-3-beta-catenin signalling. *Oncogene.* 38: 1340-1353.

Piccinini, F., T. Balassa, A. Carbonaro, A. Diosdi, T. Toth, N. Moshkov, E.A. Tasnadi, and P. Horvath. 2020. Software tools for 3D nuclei segmentation and quantitative analysis in multicellular aggregates. *Computational and Structural Biotechnology Journal.* 18: 1287-1300.

Rahman, Q.B., O. locca, K. Kufta, and R.M. Shanti. Global burden of head and neck cancer. 2020. *Oral Maxillofacial Surg Clin N Am*. 32: 367-375.

Rettig, E.M., J.A. Bishop, N. Agrawal, C.H. Chung, R. Sharma, F. Zamuner, R.J. Li, W.M. Koch, J.A., Califano, T. Guo, D.A. Gaykalova, and C. Fakhry. 2018. HEY1 is expressed independent of NOTCH1 and is associated with poor prognosis in head and neck squamous cell carcinoma. *Oral Oncology.* 82: 168-175.

Rubio, A.J., A.E. Bencomo-Alvarez, J.E. Young, V.V. Velazquez, J.J. Lara, M.A. Gonzalez, and A.M. Eiring. 2021. 26S Proteasome Non-ATPase Regulatory Subunits 1 (PSMD1) and 3 (PSMD3) as Putative Targets for Cancer Prognosis and Therapy. *Cells.* 10: 2390

Salah Fararjeh, A., A. Al-Khader, M. Al-Saleem, and R. Abu Qauod. 2021. The Prognostic Significance of Proteasome 26S Subunit, Non-ATPase (PSMD) Genes for bladder urothelial carcinoma patients. *Cancer Inform.* 20: 1-10.

Salo, T., M. Sutinen, E. H. Apu, E. Sundquist, N.K. Cervigne, C.E. de Oliveira, S.U. Akram, S. Ohlmeier, F.Suomi, L. Eklund, P. Juusela, P. Åström, C.C. Bitu, M. Santala,

K. Savolainen, J. Korvala, A.F. Paes Leme, and R.D. Coletta. 2015. A novel human leiomyoma tissue derived matrix for cell culture studies. *BMC Cancer.* 15. 981.

Shah, P., C.F. Huang, Q.L. Huang, Q.L. Li, S.A. Kazi, L.A. Byers, J. Wang, F.M. Johnson, and M.J. Frederick. 2020. Notch1 signalling in head and neck squamous cell carcinoma. *Cells.* 9: 2677.

Shhyam, M. 2015. The tumour suppressor Notch inhibits head and neck squamous cell carcinoma (HNSCC) tumour growth and progression by modulating proto-oncogenes AXL and CTNNAL1 (α-CATULIN). *The University of Texas MD Anderson Cancer Center UTHealth Graduate School of Biomedical Sciences Dissertations and Theses (Open Access)*. 638.

Son, H., A. and A. Moon. 2010. Epithelial-mesenchymal transition and cell invasion. *Toxicological research.* 26(4): 245-252.

Sun, W., D.A. Gaykalova, M.F. Ochs, E. Mambo, D. Arnaoutakis, Y. Liu, M. Loyo, N. Agrawal, J. Howard, R. Li, S. Ahn, E. Fertig, D. Sidransky, J. Houghton, K. Buddavarapu, T. Sanford, A. Choudhary, W. Darden, A. Adai, G. Latham, J. Bishop, R. Sharma, W.H. Westra, P. Hennessey, C.H. Chung, and J.A. Califano. 2014. Activation of the NOTCH pathway in head and neck cancer. *Cancer Res.* 74(4): 1091-1104.

Tan, Y., Y. Jin, X. Wu, and Z. Ren. 2019. PSMD1 and PSMD2 regulate HepG2 cell proliferation and apoptosis via modulating cellular lipid droplet metabolism. *BMC Mol Biol.* 20: 24.

Tanaka, K. 2009. The proteasome: overview of structure and functions. *Proc. Jpn. Acad. Ser. B Phys. Biol. Sci.* 85: 12-36.

Tuomainen, K., A. Hyytiäinen, A. Al-Samadi, P. Ianevski, A. Ianevski, S. Potdar, L. Turunen, J. Saarela, S. Kuznetsov, W. Wahbi, M. Risteli, A. Mäkitie, O. Monni, and T. Salo. 2021. High-throughput compound screening identifies navitoclax combined with irradiation as a candidate therapy for HPV-negative head and neck squamous cell carcinoma. *Scientific Reports.* 11: 14755.

Tuomainen, K. A. Al-Samadi, S. Potdar, L. Turunen, M. Turunen, P.R. Karhemo, P. Bergman, M. Risteli, P. Åström, R. Tiikkaja, R. Grenman, K. Wennerberg, O. Monni, and T. Salo. 2020. Human tumour-derived matrix improves the predictability of head and neck cancer drug testing. *Cancers.* 12, 92.

Ungerbäck, J., N. Elander, J. Grünberg, M. Sigvardsson, and P. Söderkvist. 2011. The Notch-2 gene is regulated by Wnt signalling in cultured colorectal cancer cells. *PLoS ONE*. 6(3): e17957.

Wahbi, W., E. Naakka, K. Tuomainen, I. Suleymanova, A. Arpalahti, I. Miinalainen, J. Vaananen, R. Grenman, O. Monni, A. Al-Samadi, and T. Salo. 2022. The critical effects of matrices on cultured carcinoma cells: human tumour-derived matrix promotes cell invasive properties. *Manuscript.*

Wang, J. J. Li, L. Zhang, Y. Qin, F. Zhang, R. Hu, H. Chen, Y. Tian, Z. Liu, Y. Tian, and X. Zhang. 2021. Comprehensive analysis of ubiquitin-proteasome system genes related to prognosis and immunosuppression in head and neck squamous cell carcinoma. *AGING*. 13: 20277-20301.

Wang, Y., W. Wu, M. Zhu, C. Wang, W. Shen, Y. Cheng, L. Geng, Z. Li, J. Zhang, J. Dai, H. Ma, L. Chen, Z. Hu, G. Jin, and H. Shen. 2018. Integrating expression-related

SNPs into genome-wide gene- and pathway-based analyses identified novel lung cancer susceptibility genes. *Int J Cancer.* 142(8): 1602-1610.

Wu, H.T., W.T. Chen, G.W. Li, J.X. Shen, Q.Q. Ye, M.L. Zhang, W.J. chen, and J. Liu. 2020. Analysis of the differentially expressed genes induced by Cisplatin resistance in oral squamous cell carcinomas and their interaction. *Frontiers in Genetics.* 10: 1328.

Zhao, Q., K. Zhuang, K. Han, H. Tang, Y. Wang, W. Si, and Z. Yang. 2020. Silencing DVL3 defeats MTX resistance and attenuates stemness via Notch signalling pathway in colorectal cancer. *Pathology – Research and Practice.* 216: 152964.

Zhou, P., B. Li, F. Liu, M. Zhang, Q. Wang, Y. Liu, Y. Yao, and D. Li. 2017. The epithelial to mesenchymal transition (EMT) and cancer stem cells: implication for treatment resistance in pancreatic cancer. *Mol Cancer.* 16(1): 52.

Åkerfelt, M., M. Toriseva, and M. Nees. 2017. Quantitative phenotypic image analysis of three-dimensional organotypic cultures. In: *3D Cell Culture* (edited by Koledova Z). pp.433-445. Humana Press, New York.

Åkerfelt, M., N. Bayramoglu, S. Robinson, M. Toriseva, H.P. Schukov, V. Härmä, J. Virtanen, R. Sormunen, M. Kaakinen, J. Kannala, L. Eklund, J. Heikkilä, and M. Nees. 2015. Automated tracking of tumour-stroma morphology in microtissues identifies functional target within the tumour microenvironment for therapeutic intervention. *Oncotarget.* 6(30): 30035-30056.

9. APPENDICES

I. NOTCH3 mRNA expression in UT-SCC cell lines by qPCR. Data are normalized to GAPDH and presented as mean ± s.d. n = 3.

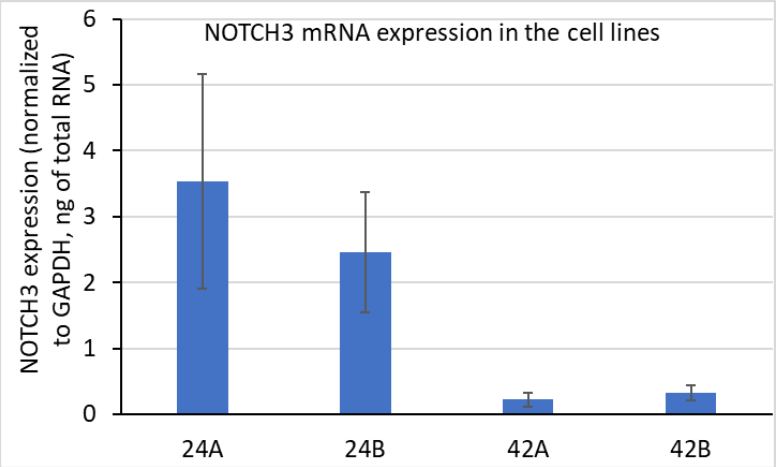

II. Representative live cell images for FLI 06 treated UT-SCC 42A in 2D culture measured by IncuCyte. The images shown here were taken before the drug was added (Day1) and after 24h (Day2), 48h (Day3), and 72h (Day4) of drug treatment. The cells were plated on day 0, and the drug was added on day 1.

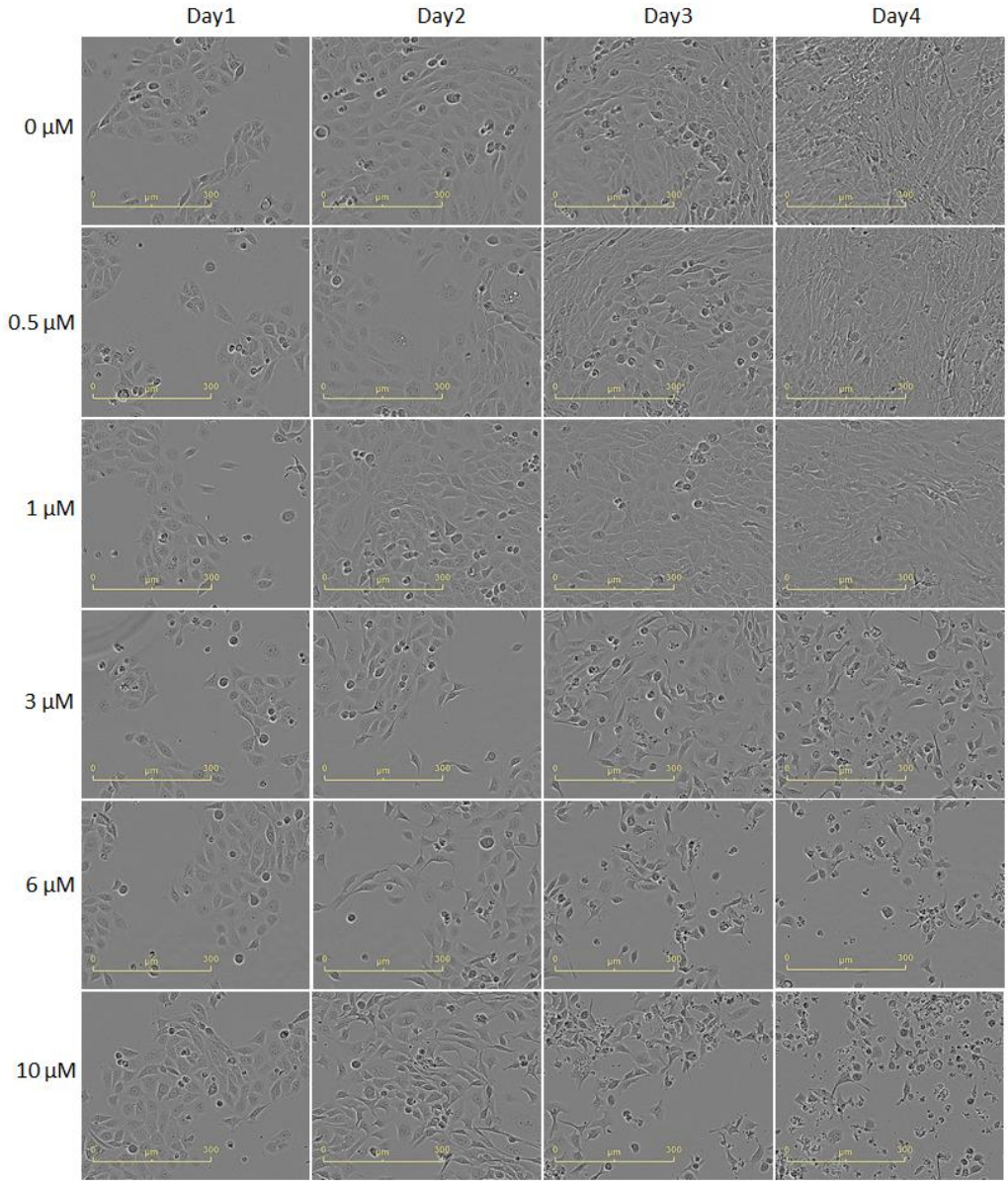

III. Effect of Yhhu 3792 on Notch activity. Quantification of western blot results. Protein expression levels was normalized to β-actin.

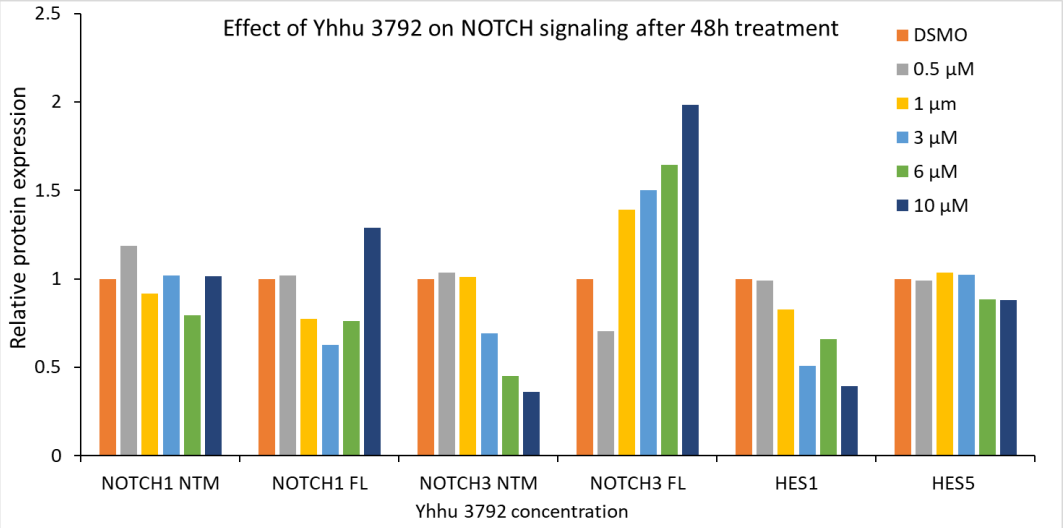

IV. Representative live cell images for Yhhu 3792 treated UT-SCC 42A in 2D culture measured by IncuCyte. The images were taken before the drug was added (Day1), after 24h (Day2), 48h (Day3), and 72h (Day4) of drug treatment. The cells were seeded on day 0, and drug was added on day 1.

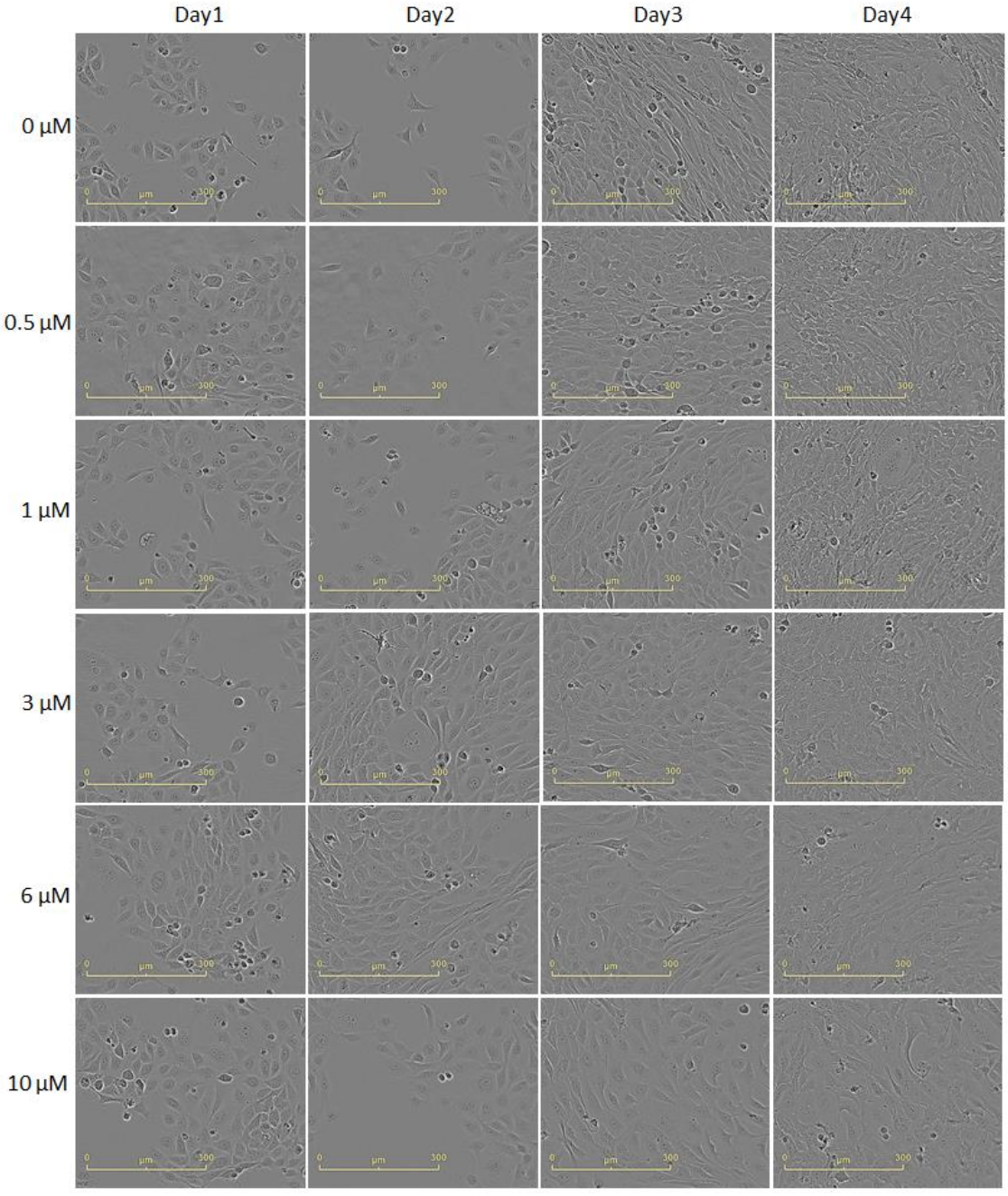

V. The representative live cell images for Yhhu 3792 treated UT-SCC 42A in Matrigel in 3D culture by IncuCyte. The images shown here were taken before the drug was added (Day 4), and every 24h for a period of 6 days (Day 5-10). The cells were plated on day 0. The drug was added on day 4.

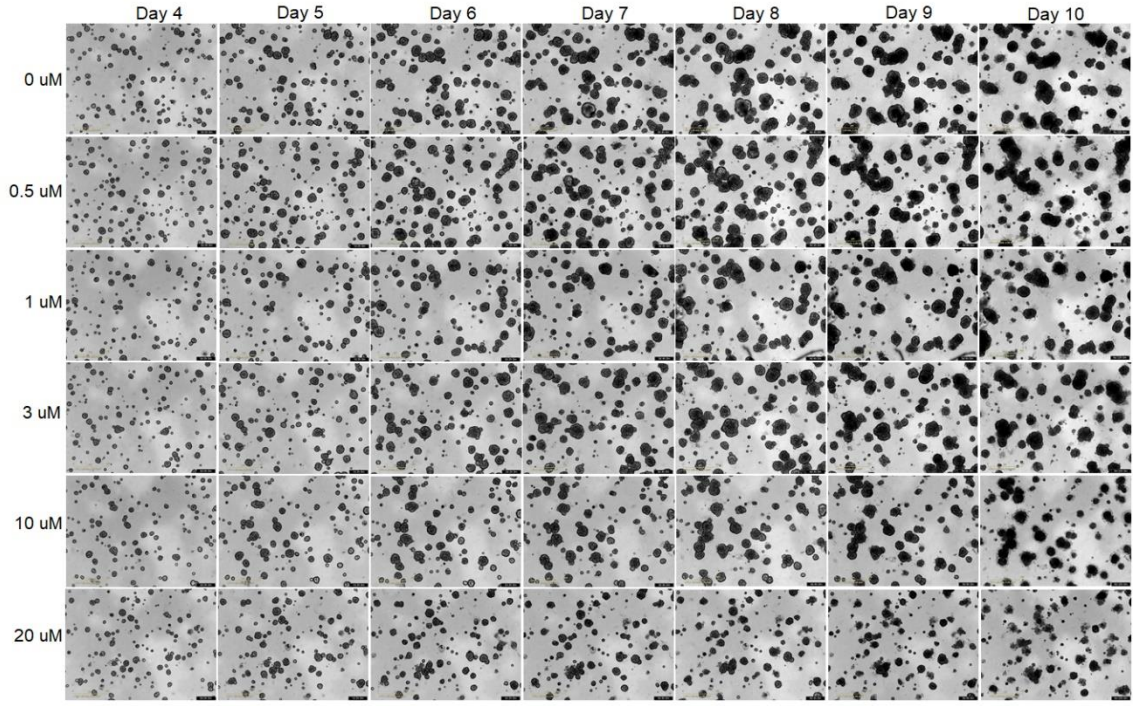

VI. The representative live cell images for Yhhu 3792 treated UT-SCC 42A in Myogel in 3D culture measured by IncuCyte. The images shown here were taken before the drug was added (Day 4), after 24h (Day 5), 48h (Day 6) and 72h (Day 7) of drug treatment. The cells were plated on day 0, and the drug was added on day 4.

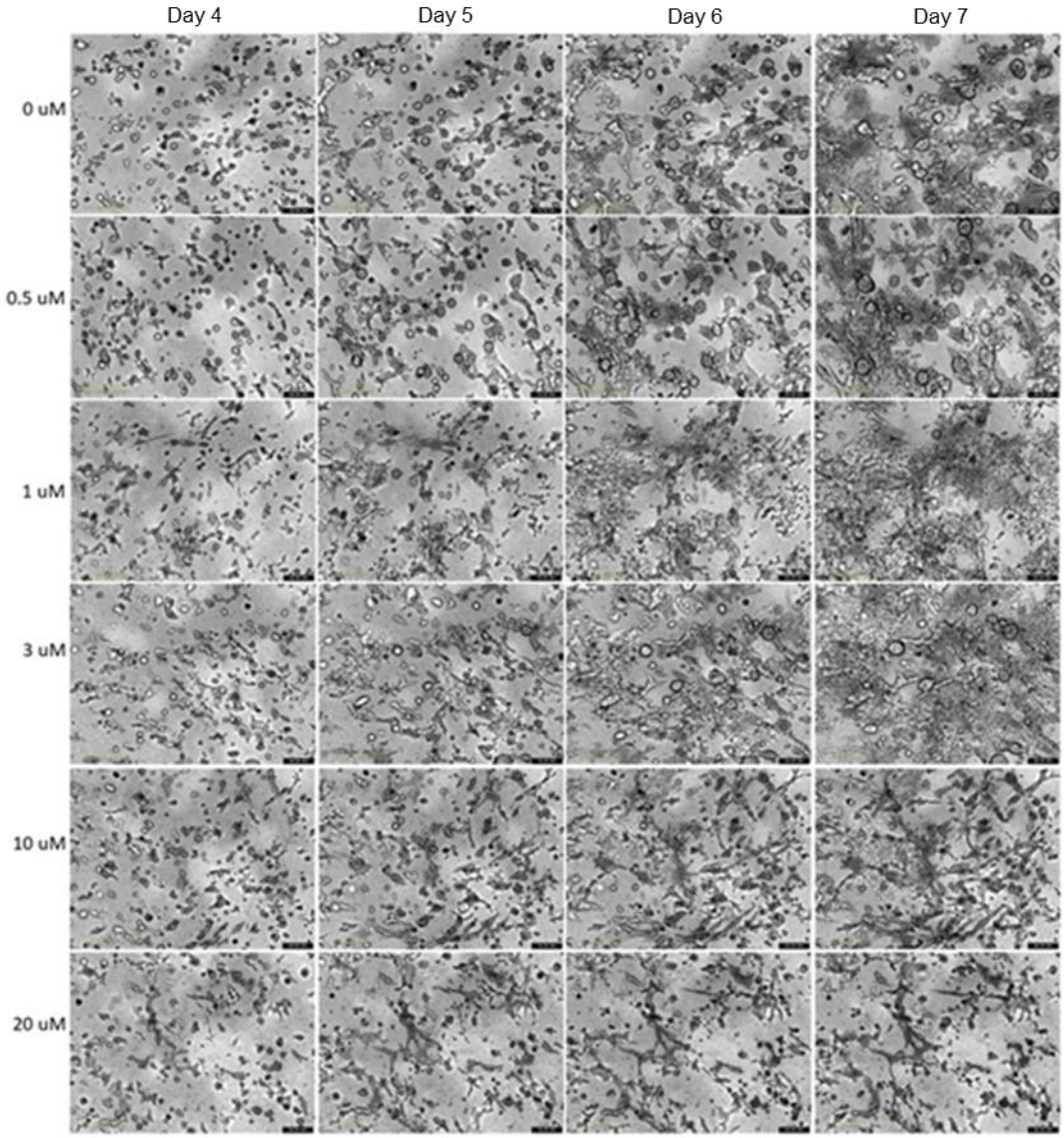

VII. Quantification of western blot results for DVL3 and NOTCH1 expression in controls and DVL3 siRNA transfected UT-SCC-42A cells after 48h and 72h transfection.

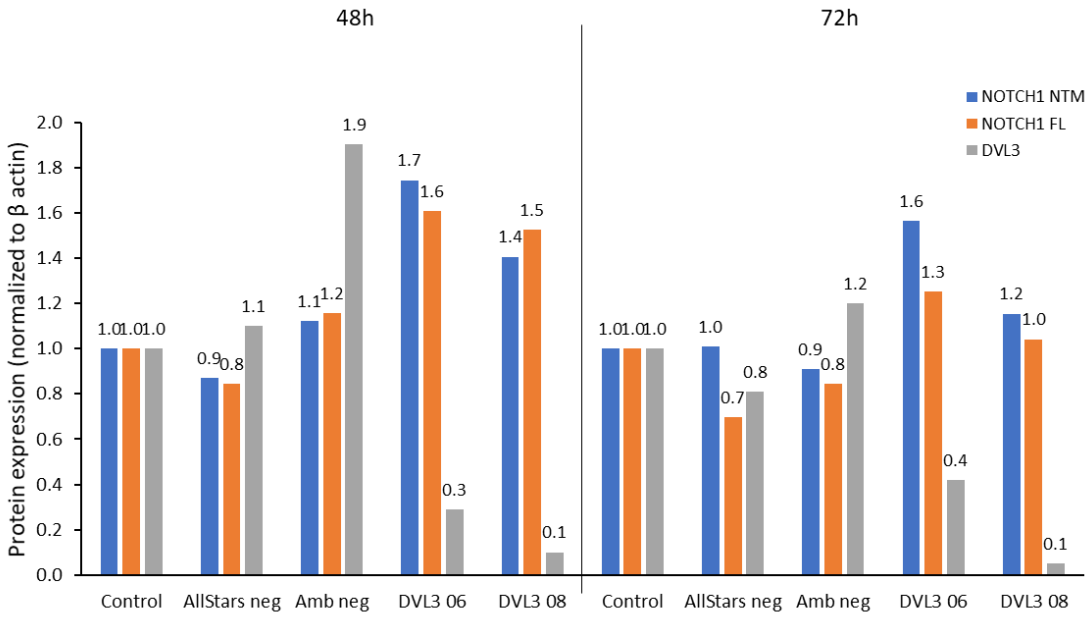

VIII. Representative live cell images measured by IncuCyte for the controls (Control, AllStars Neg, Amb Neg) and DVL3 siRNA (DVL3 06, DVL3 08) transfected UT-SCC 42A cells in 2D culture. The images were taken after 24h, 48h and 72h of transfection.